ASSESSMENT AND OPTIMISATION TECHNIQUES FOR AN ELECTRICAL IMPEDANCE MAMMOGRAPHY SYSTEM

SUBMITTED FOR THE DEGREE OF MASTER OF PHILOSOPHY AT THE UNIVERSITY OF SUSSEX

Date:	**September 2013**
Author:	**Benjamin Lingham**
Supervisor:	**Dr David Li**
Research Group:	**Biomedical Engineering**
Department:	**Engineering and Design**

Project Summary

Breast cancer detection through the use of Electrical Impedance Tomography (EIT) has been proposed for a number of years. Typically in an EIT or when in use in breast cancer detection, Electrical Impedance Mammography (EIM) system, the patient interface is that of electrodes. Positive and negative sinusoidal signals are injected into a patient multiple times at multiple frequencies, recording the developed surface voltages that naturally develop from the impedance of the body. A 2D or 3D reconstruction and visualisation of the impedance distribution is possible through the use of the recorded voltage amplitude and phase. Higher resolution images are achieved through higher electrode density (i.e. smaller electrode distance). Furthermore, tissue has a characteristic frequency response, which can be recorded if different injection frequencies are utilised. The higher the frequency, the deeper the signal can penetrate into tissue and deeper through the cellular structures, potentially leading to tissue characterisation through its frequency response.

Our group has suggested a unique combined EIT and ultrasound multimodal imaging system to detect breast cancer. This will use an EIT system to initially scan the breast, combining this parametric data with the high-resolution images of ultrasound to give a more accurate diagnosis. The prototype, known as V2, was functional but performed poorly, especially with respect to the signal to noise ratio. Images generated with this system were unclear. My role within the group was to analyze the performance of the V2 system and research best practice methods to improve the existing design, taking into consideration the intricacies of EIT hardware design and the targeted application. The improvements I suggested were incorporated into the V3 system, which was then compared with the V2 system, and showed significant performance improvement.

Contents

Acknowledgements

I would like to convey my appreciation to Dr. Wei Wang, who offered me the opportunity to join the Biomedical Engineering Research group. My thanks also go to all the members of the group for all their support during the project. I would especially like to thank Dr Nicolas Huber for his help and guidance which was invaluable throughout my time at the University. Finally I would like to thank Dr David Li for his advice when it came time to write this thesis.

1.0 Introduction

1.1 The clinical need

Breast cancer is the most common cancer in women worldwide, with an estimated 1,443,421 new cases diagnosed and an estimated mortality rate of 478,888 in 2010 [1]. In the United States alone it is estimated that in 2012 226,870 women will have been diagnosed with breast cancer and 39,510 will die from the disease [2]. It is widely believed that treatment at an earlier stage of cancer progression will reduce breast cancer mortality making early detection crucial in fighting breast cancer. Currently mammography is the most common method used for breast cancer detection.

1.2 Characteristics of breast cancer cells

Breast cancer is an uncontrolled growth of cells originating from breast tissue due to mutations, or abnormal changes in the genes responsible for regulating the growth of cells, forming a mass called a tumour. A tumour has an increased electrical conductivity compared to normal tissue due to higher cellular water and salt content. [3] This increased electrical conductivity is the characteristic that the EIM system is designed to detect.

1.3 Existing modalities

Essentially a mammogram is a low-dose (0.1 to 0.2 rad per image) x-ray system which concentrates on breast imaging. The breast is compressed against a platform exposing the breast to a small dose of ionizing radiation to produce even images at multiple angles. The images are then produced either on film or digitally [4]. There are several drawbacks to using mammography breast cancer detection. One drawback is that analysis is subjective and there can be inconsistency between radiologists [5].

It can also be harder to detect abnormalities linked with tumours in young women as they tend to have denser breast tissue [6]. Mammography lacks adequate specificity (probability that the test correctly determines there is no disease) for cancer detection, which can cause both false-positive and false-negative results [7]. A false-positive result is where the biopsy tissue is in fact benign. As much as 75% of all breast lesions that are biopsied turn out to be benign. A false-negative result is where screening fails to detect a cancerous tumour, this can happen in 5% to 17% of cases [5].

Another drawback is that the high cost of the mammography does not allow for widespread use in developing countries where there was an estimated 691,521 new cases diagnosed and an estimated mortality rate of 269,048 in 2008 [1]. The Electrical impedance mammography system described within this paper is a relatively cheap technology by comparison costing in the region of £10,000 to £20,000.

This system is non invasive and does not expose the breast to ionizing radiation, which can damage breast tissue. Currently both Magnetic Resonance Imaging (MRI) and Ultrasound are recommended for use in addition to mammography in women under the age of 40 years for whom mammography is less sensitive due to having denser breast tissue or for women with approximately 20% to 25% or greater lifetime risk of breast cancer [8].

Magnetic Resonance Imaging does have a high sensitivity (probability that the test correctly identifies the disease) for cancer detection which has generally been greater than 90% but with varying estimates to its specificity. Commonly longer acquisition times are required for higher resolution but this gives a reduction in specificity. Compared with mammography it is more time-consuming and expensive and the examination can be uncomfortable for the patient [9].

Initially ultrasound's use in breast cancer detection was to differentiate between cystic and solid lesions. This then progressed to distinguishing between benign and malignant solid lesions and can now detect microcalcifications by assessing the vascularity of tumours. [5]. One drawback of ultrasound is that the quality of the examination and analysis of results are relative to the skills of the operator and the equipment being used, and can therefore vary [10].

1.4 Electrical Impedance Mammography

The use of EIM in combination with other imaging modalities has previously been put forward [11] such as x-ray mammography [12] and in the case of our group, ultrasound. Our group has built a unique non invasive combined EIM and ultrasound multimodal imaging system to detect breast cancer. This will use an EIM system to initially scan the breast, combining this parametric data with the high-resolution images of ultrasound to give a more accurate diagnosis. This system does not expose the breast to ionizing radiation like mammography which can be damaging to breast tissue.

1.5 The development of EIT and EIM

In 1664 Robert Hooke discovered cells whilst looking at thin slices of cork under a microscope [13]. 185 years later Peltier recorded that cells from tissue have capacitance and can store electrical energy [14]. Hermann observed in 1872 that the electrical resistance measured across freshly excised muscle taken from a frog was approximately 7 times that of the resistance when measuring along the same muscle as the muscle died [15]. Crucially for the theory of Electrical Impedance Tomography (EIT) this was followed in 1923 when Grant found that tumour cells had a lower resistivity compared to normal cells at low frequency [16]. Shortly after, Fricke and Morse found significant difference of capacitance between malignant breast tumours and normal tissues [17].

Further research on resistivity was carried out by Geddes and Baker (1967), who reviewed the emerging research into the resistance of tissues and the electrical resistivity of blood, other bodily fluids, cardiac muscle, skeletal muscle, lung, kidney, liver, spleen, pancreas, nervous tissue, fat, bone, and other miscellaneous tissues [18]. In 1975, Denniston and Baker used electrode arrays to measure changes in the electrical impedance of the thorax. They infused and withdrew saline, plasma, or blood from the right, left, or both hemithoraxes and discovered that there was a linear correlation in impedance changes with the volume of infused fluid [19].

Three years later, Henderson and Webster designed and built a system which they called an impedance camera to produce electrical impedance images of the thorax [20]. Then in 1984 the first practical medical EIT system was created at Sheffeld University by David Barber and Brian Brown. The system comprised of 16 electrodes and applied a constant AC current at 50kHz. They used the back projection method to generate what is generally regarded as the first successful EIT vivo Image [21]. The Sheffield research group were also the first to build a clinical EIT system [22].

Since then many research groups have worked on EIT, increasing its potential and number of applications in the field. EIT has been used to image many other areas including brain [23] lung [24-26], heart [27] and used to assess human body composition [28]. It has also been used to for abdominal EIT and to detect acute intra-abdominal haemorrhage [29, 30] as well as cellular images [31-34]. However we are concerned with breast EIT. [35-43].

1.6 The Theory of EIT

The most common EIT system injects an AC current into the patient through electrodes. This is because biological tissue is an ionic conductor, meaning electrical charge is passed though free ions in suspension in solutions, if a direct current is passed through an ionized solution, it will cause the electrodes to polarize. In effect what occurs is as the current passes a double layer of ions is quickly deposited at each electrode which acts as an insulator and prevents the current from passing [44]

The system will then read back the developed potential difference through other surrounding electrodes. This process can be repeated a number of times over a range of frequencies with different electrodes driving and receiving. The measured developed potential differences are then read back and the voltage and in some cases phase shift of these voltages are used to build a 2D or 3D image of the analysed area. This process is often referred to as the forward and inverse problems.

The EIT forward problem is to determine the developed potential difference on the surface of the analyzed area, given the conductivity or permittivity distribution inside the analyzed subject area by injecting a known signal current source or voltage.

The inverse problem is to reconstruct an image by fitting the forward model to the conductivity or permittivity measurements made during the scan. There have been several image reconstruction algorithms developed for this purpose.

Different frequencies aid in measuring different depths of tissue. Our groups system works between 100Hz and 10MHz with a constant 1mA AC current at 1mV peak to peak. The higher the frequency the deeper the signal can penetrate into tissue as higher frequencies can penetrate the cells easier than the lower frequencies and therefore uses less energy travelling to the same destination. A representation of this is shown in *Fig 1.0* where the line representing the lower frequencies takes a longer route around the cells to arrive at the same point as the line representing the higher frequencies, which passes through the cells. [44]

Fig 1.0 shows the path higher and lower frequencies take through tissue. On the left lower frequency signal takes the longer route around the capacitive components of the tissue and on the right the signal passes through the capacitive tissue

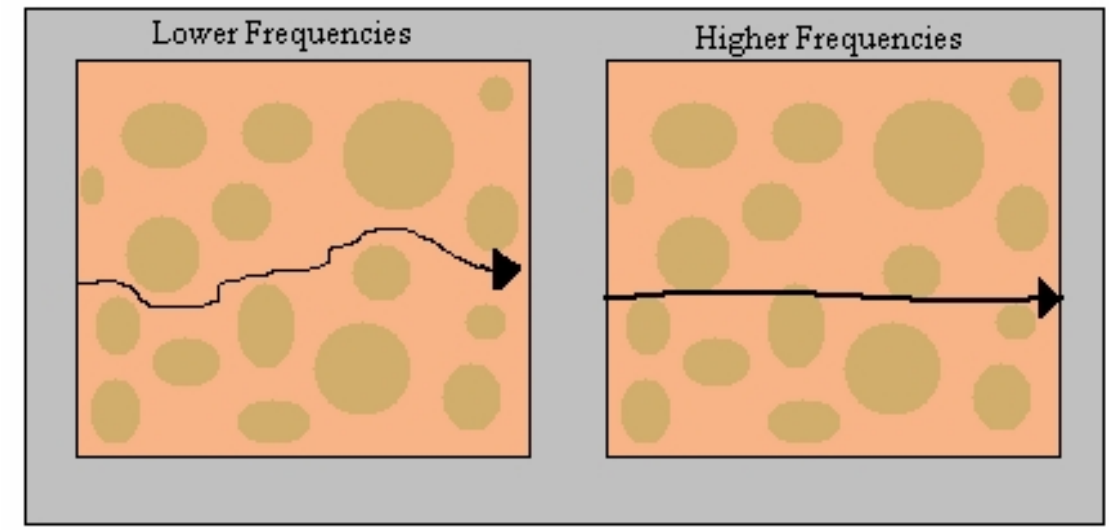

Biological tissue is comprised of a mixture of resistive and capacitive components. The resistive components will allow current to pass regardless of frequency whereas the capacitive component will only allow the higher frequency current to pass as represented in *Fig1.1* [44]

Fig 1.1 Shows a representation of the resistive and capacitive components of biological tissue. The lower frequency signal can only take the longer resistive path whereas the higher frequency signal can take CR path

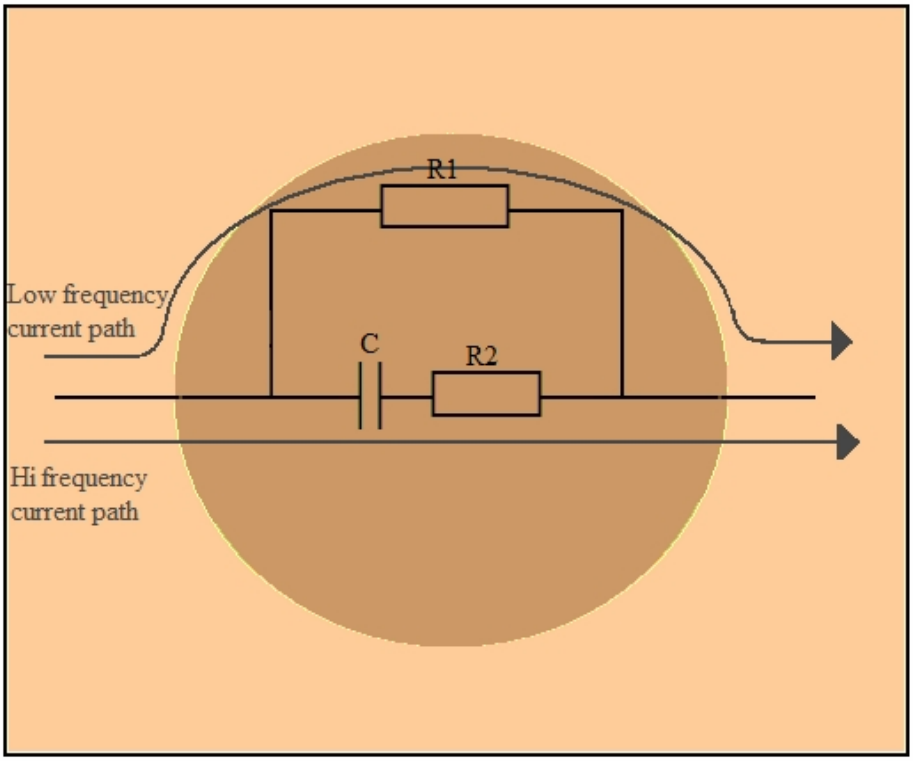

Frequencies below 10Khz take the path through R1 at around 10kHz current begins to penetrate the outside layers of the cell and as the frequency increases between 10 kHz and 500 kHz the current takes more and more the path through C+R2. As the frequency increases further the effect of the capacitance is nullified until full penetration occurs over 1MHz [44]

As a general rule a sinusoidal current travelling between two electrodes will travel to a depth of about half the distance between the two electrodes. This however will vary dependant on the frequency, as previously stated the higher the frequency the better the signals will penetrate through the tissues of the subject under test. This is represented in *Fig 1.2* [45]

Fig 1.2 Shows how distance and frequency affect the depth that the signal can penetrate. The higher the frequency the deeper the signal can penetrate

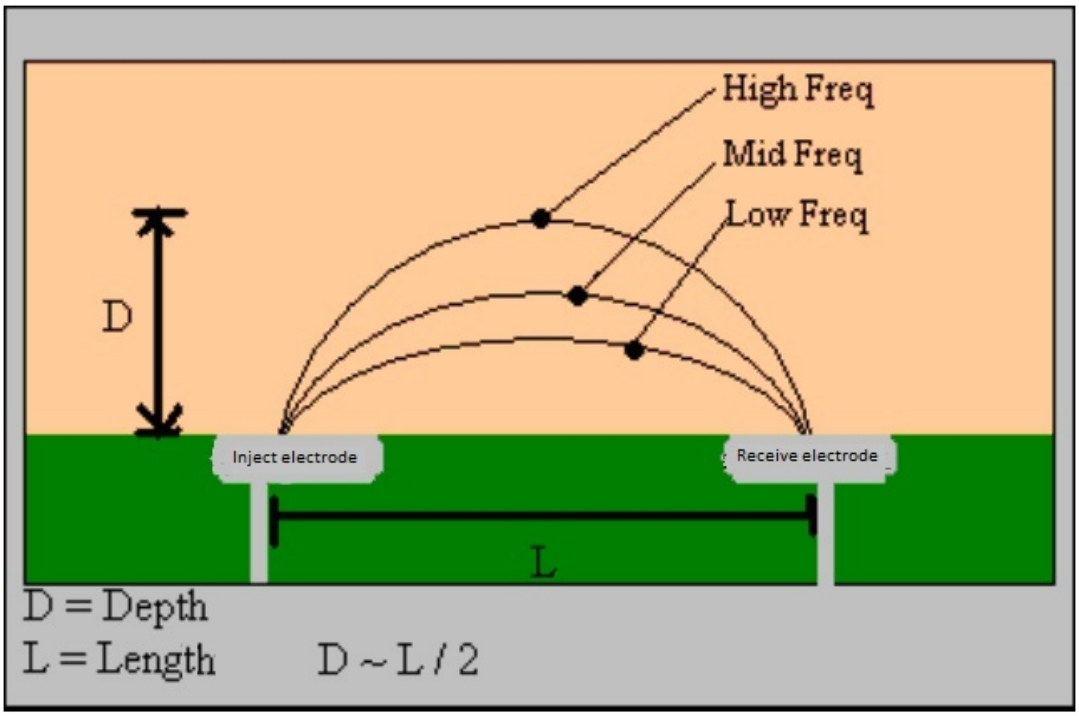

To build up a 3D image the system uses a combination of increasing frequencies and different 'receive' electrodes spaced at increasing distances from the 'inject' electrode. This is represented in *Fig 1.3*

Fig 1.3 Shows how a combination of distance and frequency affect the depth a signal can penetrate increased distance combined with higher frequency will increase the depth the signal can penetrate

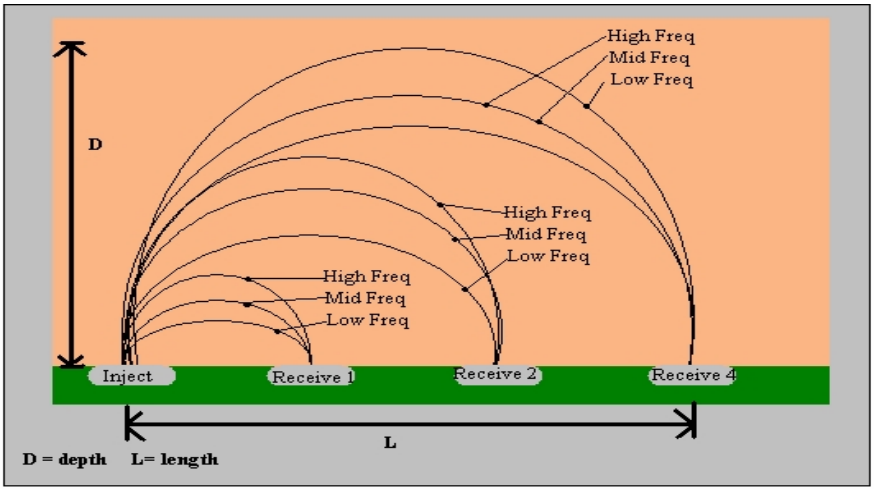

A tumour is denser than normal tissue as its cells are packed closer together; it is also less resistive and capacitive. When the signal passes the cancer cells it affects the voltage differently to when it passes normal tissue. It also changes the time it takes for the signal to reach the receive electrode, which causes changes in the phase. It is these differences that are used to build up the final images [46].

1.6.1 Two Electrode systems

The two electrode system uses two electrodes which when in contact with a patient form a current carrying circuit. One electrode will act as a sense electrode and the second as counter electrode. An AC signal is applied between the sense and counter electrodes and the resultant voltage measured including the effect of the sense/counter electrode and impedances from the measured area of the patient. There are two types of two electrode systems each having different electrical properties. One type uses two non-polarizable electrodes and the other uses two polarizable electrodes.

1.6.1.1 Polarizable Electrodes System

The polarizable electrodes system uses two polarizable electrodes. When current is applied to an ideal polarizable electrode no actual charge crosses the electrode-patient interface. The current across the interface is a displacement current and the electrode behaves like a capacitor. Large changes of electric potential of the electrode are generated from minor changes in current. A polarizable two electrodes system is best used for applying a potential difference across the measured area of the patient. [47][48].

1.6.1.2 Non-polarizable Electrodes System

"Ideal non-polarizable electrodes allow current to pass freely through the electrode-patient interface requiring no energy to make the transition and producing no change in electric potential" [48]. A non-polarizable two electrodes system is best used for measuring the potential differences in two phases, across the measured area of the patient, or for passing a large current through a measuring system. [47]. This two electrode system is the one generally used for EIM. Common types of electrode used for EIM are Ag/AgCl electrodes. Unfortunately no non-polarizable electrodes are ideal although they can approach it at lower currents. As a result, when current passes through the measured area of the patient the potential at the counter electrode interface varies.

1.6.2 Three Electrode system

With the three electrode system the problem of varying potential and the counter/patient interface is overcome by measuring the potential changes of the sense electrode independently of changes that may occur at the counter electrode. This is achieved by dividing the counter electrode into reference (which has no current flow and no polarization) and auxiliary electrodes. The current flows between the sense and auxiliary electrodes and by measuring the potential reference voltage with respect to sense the admittance of sense is calculated and performed in the system by operational amplifier in a constant voltage, admittance reading circuit As shown in *Fig 1.4* [49] [50].

Fig 1.4 The 3 electrode system demonstrating current flowing between sense and auxiliary electrodes and a reference using the reference electrode to calculate admittance

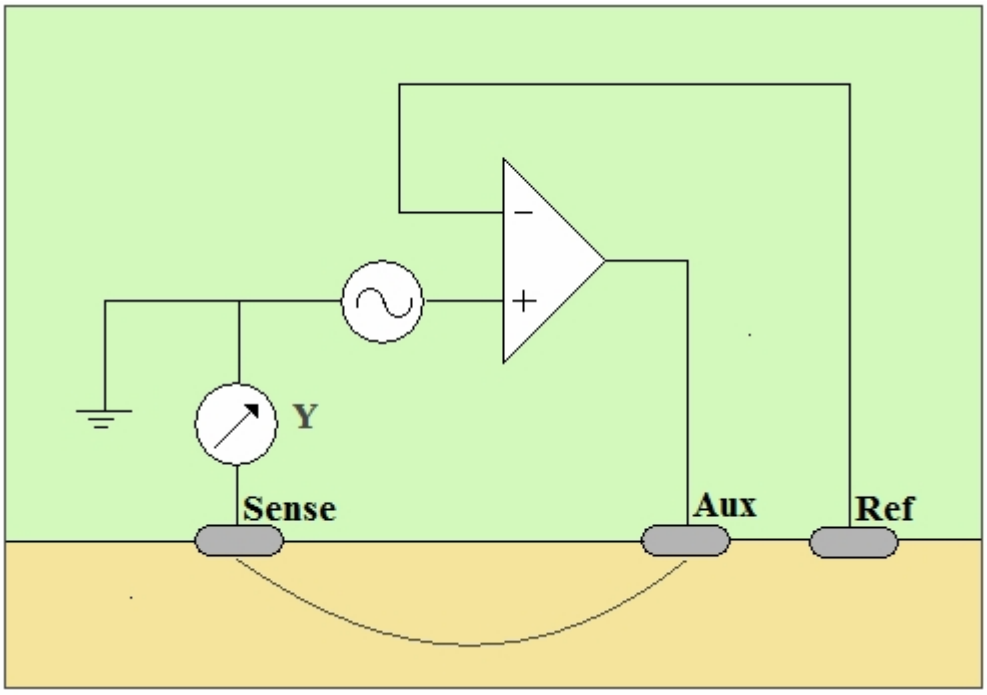

1.6.3 Four Electrode system

The four electrode system is the most widely used EIT measurement method and uses separate pairs of current-carrying and voltage-sensing electrodes. Constant current is applied between the outer pair of electrodes and the resultant electrical potential is recorded between the inner electrodes; this overcomes the electrode impedance issues and contact resistances that occur in the two electrode system. Almost no current flows in the sense so the voltage drop is particularly low making the system more accurate [21].

Fig 1.5 The 4 Electrode System demonstrating current applied between the outer pair of electrodes and voltage measured at the inner electrodes

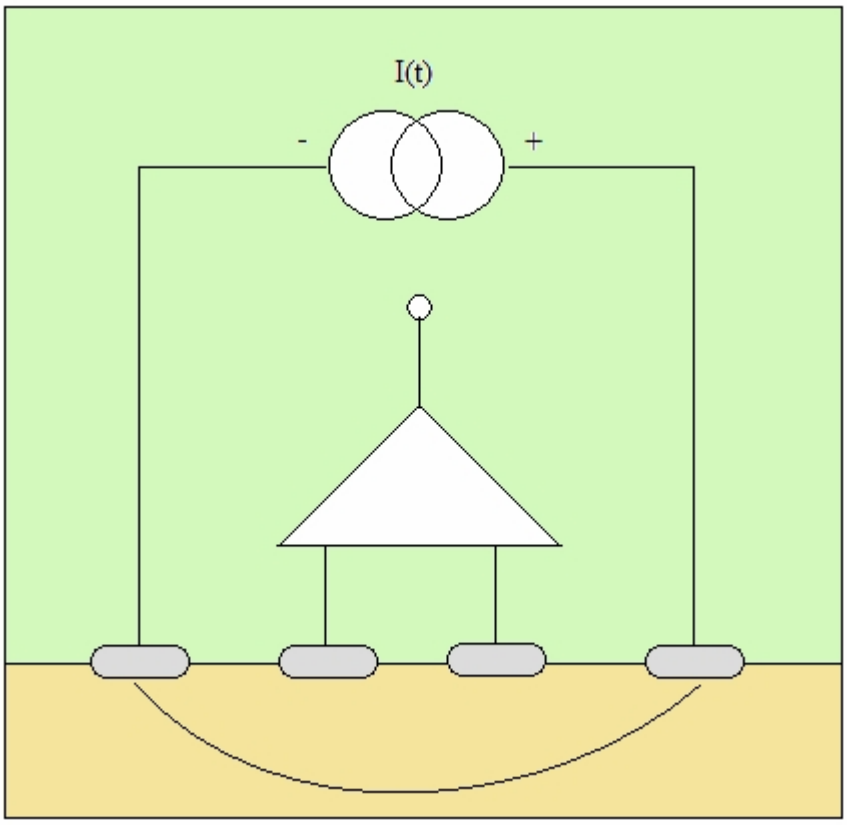

1.7 Other EIM Research Groups

1.7.1 The Israel research group

Piperno *et al* from the Israel research group designed a 2D planar array EIT system for breast cancer detection which became known as T-SCAN™. The T-SCAN™ system has 3 different arrangements of hand held electrode arrays. There is an 8x8 rectangular grid (64 electrode) array with a footprint of 32mm by 32mm and there are two arrays with 16x16 rectangular grids (256 electrodes). One with a footprint of 32mm by 32mm and the other with a footprint of about 72 mm by 72 mm. Thanks to its interchangeable and condensed size arrays the T-SCAN™ system is apt for real time breast screening with multiple images able to be obtained and evaluated by moving the probe over areas of the breast [39] [3].

The T-SCAN™ runs at a frequency range of between 100Hz and 100kHz. A disadvantage of the condensed size arrays and the uppermost frequency of 100kHz is that the maximum depth that the system cap penetrate is only between 3 to 3.5cm. Also although at lower frequencies the system's signal-to-noise ratios is nearly 70dB at the higher end of the range it drops to 40dB which will negatively impact the reconstructed image [39]. The system works by applying an alternating electric field in-between the patient's arm and breast. The patient holds an electrode (a stainless steel cylinder) and the probe is then guided over the entire breast in a pre-defined sequence. The resulting currents are measured at each of the hand held array's individual electrodes, which are held at virtual ground.

Conductance and capacitance related maps are calculated from the measured amplitude and phase shift of these currents; from this 3x3 data sectors are recorded. When both breasts are scanned each displaying conductance and capacitance, four 3x3 sector maps are created The groups results showed that the system was unable to detect lesions behind the nipple the system would indicate a bright white spot due to decreased impedance of the nipple tissues. This makes it difficult to detect tumours that lie behind the nipple. [39] [3].

1.7.2 The Moscow research group

Cherepenin *et al* of the Moscow research group originally designed a system for breast cancer detection comprising 256 electrodes arranged in a square matrix, which injected and measured a 10kHz signal [42]. The group found that this arrangement of electrodes had areas where the electrodes had little contact with a patient so re-designed the layout to substantially increase the area of contact. The new design was a 3D planar array EIT.

The system has a circle-shaped array also comprising of 256 electrodes. Similar to the Israeli system this system also has an electrode connected to the arm in this case two remote electrodes are attached via a clip to the wrist. One electrode acts as a common AC current source and the other as a reference electrode used to detect the potential difference.

To increase the number of electrodes in contact with the breast the flat surface of the electrode array is pressed up against the breast, flattening it toward the chest with tap water is used for moistening the skin [51]. The system runs at a frequency range of between 10kHz and 50kHz and the output from the AC current source is switched to activate each electrode in the array, while the second remote electrode is constantly on. The difference between the selected electrodes is measured by a potential difference detector and uses the extended back projection algorithm method for the 3D image reconstruction of 7 cross sections added together [42][51][52].

The group tested the performance of their system using a dielectric tank filled with water containing immersed test objects. The tests showed consistent image results with regards resolution and sensitivity up to 60kHz, however at frequencies greater than 60kHz artefacts started to affect the image.

Attempts were made to improve the image quality by increasing the resolution time but with no improvement. The group determined that these artefacts were caused by systematic errors which they put down to crosstalk. They therefore chose 50kHz as the maximum frequency of the system. Having 50kHz as the maximum operating frequency severely limits the ability of the system as at 50kHz the signal is only just starting to penetrate the exterior of the cell wall. This limits the tumour detecting capabilities of the system and the depth to witch it will be able to measure [51].

1.7.3 The Rensselaer Polytechnic Institute research group

In 1989 Cheng *et al* introduced the complete electrode model for an EIT system at the Rensselaer Polytechnic Institute. The research group went onto design a 3-D planar array EIT system for breast cancer detection known as the ACT 4 system, which is used in combination with X-ray to produce dual images for the two modalities. The system uses two sets of planar electrode arrays containing 60 radiolucent (allows X-ray photons to pass) rectangular electrodes on each side. [53][11].

The Rensselaer Polytechnic Institute uses the optimal current method meaning currents are injected through all planar electrodes into the breast and the voltages on each electrode is measured simultaneously giving uniform current distribution. This is a very good method for increasing the discernibly of malignant tumours from healthy tissue [53][11].

Voltages and currents can be applied over 6 frequencies ranging from 3kHz and 1MHz to each of these electrodes and the resulting currents and voltages can then be measured. The group's struggled to create a current source that would sustain accuracy over the systems frequency range due to the capacitance of the systems electrode array which is why the voltage measurements are necessary. Another issue with the system is that like the Israeli configuration with its condensed size arrays the system also suffers from poor depth resolution [53][11].

1.7.4 The Dartmouth research group

The first generation of Dartmouth's EIT system for breast cancer detection which was created by Hartov *et al,* and consisted of a 16 electrode circular array, which could be adjusted by rotation and along the length of the breast from chest wall to the nipple. The system worked be applying voltages and measuring the currents over a frequency range of 10kHz–1MHz [54].

The current generation of Dartmouth's EIT system consists of 64 electrodes which are arranged circularly in groups of 16 having 4 parallel planes at different distances from the patient chest. Similar to the Sussex group the Dartmouth group have an examination table with a cylindrical cavity in which electrodes are embedded. However unlike the Sussex group's flat electrode planner array Dartmouth uses stepper motors to bring electrodes which are mounted on rods into contact with the breast [55]. This system injects AC current at 10kHz, 127kHz, 1.13MHz, and 10MHz and the records the voltages [56].

The group were able to safely image 96 women and obtain the impedance spectra. Their results showed significant differences in the mean image conductivity for different tissue types with the more significant differences occurring at higher signal frequencies. The group believed that this could be a result of reduced contact impedances or because physiological variations in breast tissues are more prominent in the higher frequency range [56].

Previous testing had shown that when looking at the complete cross section of the breast the reconstructed image includes regions of apparent electrode surface artefacts and 3D data to model mismatches. These appear as a layer of low properties near the boundary of the reconstructed images. [54]

1.7.5 The Duke University research group

Kim Hwa Lim *et a*l of the Duke University research group reported results of a 2D circular electrode array EIT system for breast cancer detection that the group had designed. The system comprised of a cylindrical container housing thirty two stainless steel electrodes acting both as current source and measurement electrodes injecting and reading an AC 100kHz signal. The system would obtain two voltage readings and a current reading [43].

The group later designed a 3D system for breast cancer detection. This system combined multiple circular arrays into a cone shape with 128 electrodes arranged in seven concentric vertical tiers. The group believed that a cone-shaped EIT array offers a better profile to image breast. The array has a greater number of electrodes at the top level gradually reducing in number as the levels go down. This means that higher spatial resolution can be achieved compared to a cylindrical system because of the closer distance between electrodes and the breast. In this system each electrode can act as a current source injecting an AC 10kHz signal, measurement electrodes and can be grounded [57].

Similarly to the Sussex system the Duke University group uses the four-electrode method which has two current drive electrodes and two voltage measurement electrodes. Like the Sussex group they use a body temperature saline solution that has conductivity similar to that of normal breast tissue to help conduct the signals to and from the electrodes [58]. A known issue with a ring based electrode EIT system is the closer to the centre of the imaged region the lower the resolution the system will be able to obtain. For improved resolution at the centre of the imaged region the group selected electrode pairs in a fashion that the current flow will pass as much as possible through the centre region.

An example of this would be to select a source electrode on the uppermost level of the array while the sink electrode would be selected from the lowest level of the opposite side of the array. Initial phantom testing showed promising results from the experimental data collected, satisfactory 3D phantom tumour images were reconstructed showing good spatial information [57][58].

1.7.6 The Technical University of Gdansk

Wtorek *et a*l of the Technical University of Gdansk designed a 3D system for breast cancer detection known as the TUGEM (Technical University of Gdansk Electro-impedance Mammograph) system. This system comprises of a hemispherical ring electrode array 16cm in diameter, which is similar to the conical array of the Duke research group.

The array incorporates 64 compound electrodes fixed in four rows. Similarly to the Sussex system the Technical University of Gdansk use a saline solution to aid conductivity to subject to be analysed [59].

The system uses the 4 electrode technique and can inject current and measure the voltage or applies voltages and measure the current. To obtain the data for image reconstruction the system injects an AC current input signal over a frequency range of 10kHz to 1MHz and takes a total of 2048 linearly independent measurements and digitises the samples using a 12 bit analogue-to-digital converter [59][40].

The group conducted a phantom study using the different materials. Plexiglas aluminium and a cucumber were chosen and cut into a cylindrical shapes with a volume of 2.3%, 2% and 0.5% with respect to the electrode array container. The electrode array container was then filled with a conductive solution and the system run.

The results show that all three materials with a relative volume of 2% can be recognisable albeit with without a high contrast between the material under test and the conductive solution. A major drawback to the methods used in this system was found to be that the accuracy of the contrast depends heavily on the positioning of the material under test. [59].

2.0 Project Definition

The project was to create a breast cancer scanner using signal analysis in conjunction with the traditional ultrasound to locate tumours and display the results as a 3D image. The EIT system would initially scan the breast and then, by combining this parametric data with the high-resolution images of ultrasound, give a more accurate analysis. The project required three signal analysis prototypes to be built and one combined EIM and Ultrasound system.

The initial prototype tested that the control and signal functions can produce an image. The second refined any problems found within the first design and focused on how best to position the components and layout of the boards. The third prototype should have had any problems with signal noise and imaging eradicated. Upon joining, the project was at the second prototype stage.

The prototype known as V2 did not generate a clear reconstructed image. The main reason for this was believed to be that high levels of noise that was inherent in the system adversely affected the signal to noise ratio thereby making reconstructing a clear image of a measured object impossible. In the next generation of board to be known as V3 the issues affecting the image needed to be resolved so that a clear image could be generated with the EIT scan.

My role within the project was to take this prototype which had already been created, test and analyse its performance and based on these results define where gains could be made, then suggesting architectural improvements using best practices for the new design.

The version 2 iteration of the hardware had been laid out and manufactured by external contractors who did not release the circuit diagrams or board layout architecture. I received limited schematic documentation and the V2 hardware from which, before I started testing the hardware I would have to reverse engineer to be able to create new circuit diagrams of the circuit to work with.

2.1 A breakdown of the Sussex system

The Sussex whole system comprises of:

- An EIM System
- Ultrasound System
- A PC
- National Instruments System
- Stepper Motor

The interaction between the Sussex system components can be seen in *Fig 2.0* and interaction between the Sussex system and a patient can be seen in *Fig 2.1.*

Fig 2.0 Shows the interaction of system components. A PC runs the software and controls the NI chassis which in turn controls the hardware. Cards within the NI chassis handle the signal generation, signal digitisation, image acquisition and motor control

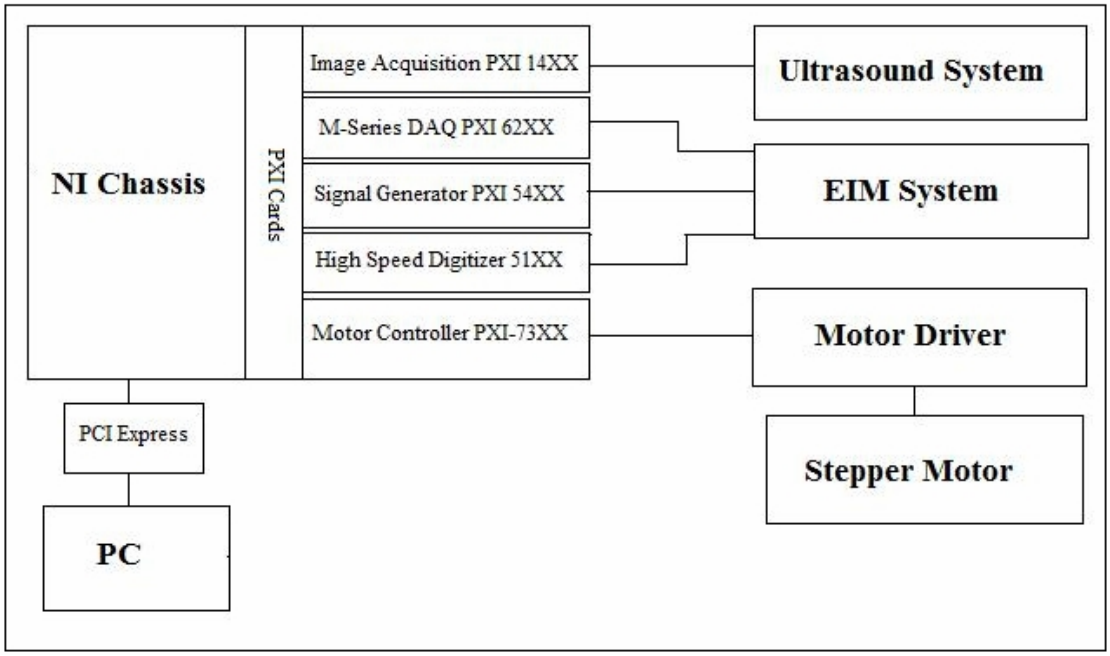

Fig 2.1 Shows the intended interaction of the final Sussex system and a patient. The patient will lie on a specially adapted table and the breast will be positioned into the EIM housing which will be filled with saline at room temperature. The EIM planar array will be raised into contact with the breast flattening the breast against it. The system will then run both an EIT and ultrasound scan

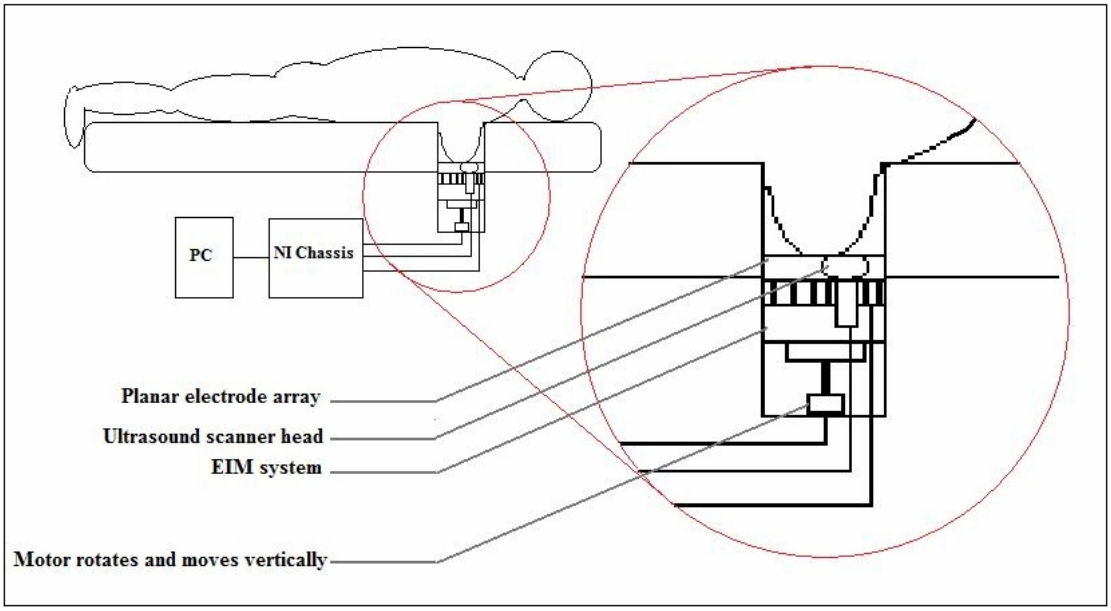

This project is focused specifically on making improvements to the EIM System, which is depicted in *Fig 2.3.* This system was based on Commercial-Off-The-Shelf (COTS) components, but also included a large number of in-house designed printed circuit boards.

2.2 A breakdown of the Sussex EIM system

The Sussex EIM system uses a 4 electrode method for impedance detection incorporating an 85 electrode planar array. Any two electrodes can be selected to apply current to the breast whilst two other electrodes that are within a selected radius of the current drive electrodes are selected to detect the developed potential.

The pattern of elected sense electrodes are chosen so only the strongest signals are read back to make up a clearer image. The system is required to operate between frequency ranges of 100Hz – 10MHz [60]. 10MHz was chosen as the maximum frequency as beyond 10MHz it becomes hard to find components that can handle the bandwidth.

The Sussex system uses the Back-Projection [61] and the Newton-Raphson based Method for reconstruction of the image. This is what is known as the inverse method. [62]. The Sussex group also customized a novel implemented mesh, regularization constraint and multiple frequency reconstruction method [63].

The Sussex MK4 EIM system comprises of:

- A main board
- A daughter board
- A digital control board
- A PC
- National Instruments System

Fig 2.3 Shows a detailed breakdown of the EIM part of the system. A sine wave is generated with the NI equipment which is then converted to a constant current on the daughter board this current signal is then switched to different electrodes on the main board and on to the planar array, the control of which is done on the digital control board. The daughter board then receives the generated surface voltages which it differentiates and is then digitized by the NI system and reconstructed on the PC

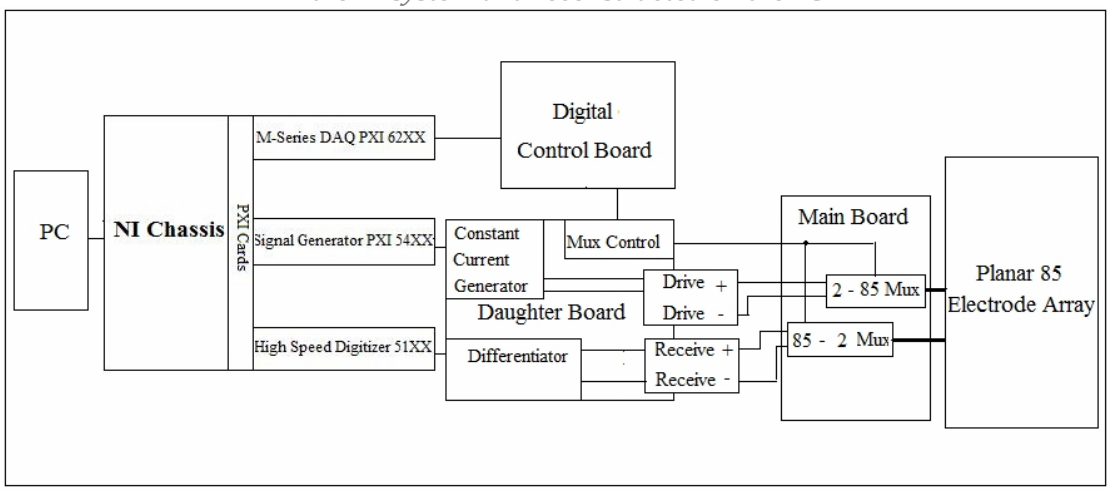

2.2.1 Main board:

The main board is where all the signal switching is done; it receives a positive and negative constant current sinusoidal signal from the daughter board and switches it through an ADG2128 device to the necessary electrodes. It simultaneously switches the signals at receiving electrodes back through an AD8114 device to the daughter board.

2.2.2 Daughter board:

The daughter board receives a sinusoidal wave from the national instrument's equipment. It then converts this signal to a positive and negative constant current signal through a VI stage, which it supplies to the main board. The daughter board also receives the digital switching data from the digital control board via a ribbon cable. The daughter board then buffers the data, which then goes to the main board and the switching device on the daughter board. The daughter board will receive the two return signals from the main board and combine them through a differentiator; the resultant output signal is connected to the national instrument's equipment.

2.2.3 Digital control board:

The digital control board is an interface between the national instruments equipment and the daughter board. It buffers the logic data for the switching devices and it selects the CE (chip enable) lines for the devices on the main board.

2.2.4 National Instruments system:

The National Instruments (NI) system comprises of a NI PXI –10XX chassis, this houses:

- An NI PXI-54XX 16 bit 40MHz function generator card.
- An NI PXI –51XX 14 bit 100MS/s Digitiser.
- An NI PXI-62XX M series multifunctional DAQ.

The NI PXI –10XX chassis also connects to the digital board via an SCB-S68 box, the NI PXI-54XX function generator delivers the range of frequencies to the daughter board. The NI PXI –51XX digitiser receives the final signal back from the daughter board and digitises the information, which is then read by the PC.

The NI PXI-6259 M series multifunctional DAQ is the interface between the national instruments system and the digital board. Each one of these cards is fixed into the NI PXI –10XX chassis, which is controlled by a PC. The digitised signal from the NI PXI –51XX card is also read into the PC, which uses the information to create its image.

2.2.5 PC:

The PC uses LabView software to control the national instrument equipment and Matlab software to construct an image from the information gained during the scan. The PC can also look at each individual signal separately on a virtual scope, which can be used for fault finding and looking at the noise levels. The PC also sends the logic that controls the switching on the boards.

2.3 Calibration

Once as much as possible has been done to reduce any noise generated by the systems hardware and screen any external noise, signal calibration is used to filter any signal noise still present in the system by using two calibration methods.

Firstly the reciprocal measurements (inverting the driving/receiving pair of electrodes, or shifting the driving and receiving electrodes to a mirrored position) are compared to the original measurements with any disparity between measurements highlighting variations in electrode performance requiring hardware adjustments. The second method uses signal noise filtering by comparison.

What this entails is taking the real and simulated measurements and comparing them, if there is any disparity linear to changes in frequency and loading then signal processing can be used to assist calibration and improve accuracy. Non linear disparity will require hardware adjustment [63].

2.4 Project information

The project was to re-design the V2 prototype and create and manufacture a V3 prototype, eliminating any inherent issues in the previous design. The V2 prototype was originally designed and built by the project team, who are made up of research and design engineers, not manufacturers. The project team reported that they were unable to reconstruct a clear scanned image.

This was mainly due to too much noise within the circuit. The signal to noise ratio (SNR) was so poor that the reconstructed image contained a large amount of artefacts which made it impossible to differentiate the object being scanned from the background.

Apart from potential issues caused by possible poor design and or layout of the PCB the noise problems may have been compounded by the fact that the boards had been hand populated without using best practice manufacturing techniques. There appeared to be potential dry joints and general poor soldering.

The first thing I did was to have the V2 boards professionally built, using best practice manufacturing to eliminate possible build issues as contributing factor to poor results. These new V2 boards will then be used as the standard by which any modifications are compared.

2.5 Project Specification

Firstly a new V2 prototype had to be built professionally and then evaluated. Using the information gained from testing the new V2 prototype, research and investigation into improvements had to be performed. The prototype then had to be redesigned.

The board must have an improved SNR and be able to produce a clear reconstructed image of a scanned object. No specific target SNR value was given by the project team. However the best SNR that the NI equipment being used would be able to achieve in the system would be 60dB. Therefore 60dB was my target to achieve the best clearest possible image from a full scan of an object.

The SNR of the professionally manufactured V2 prototype had not been ascertained at this point; however the perception was that it would still be poor. The same manufacturer and component types were chosen as used on the V2 prototype populated by the project team. New V2 main and daughter PCBs needed to be created. These boards are both two-layer boards, which mean they only have tracking on the two outside surfaces and have no inner layers. The tracking was left the same for these new V2 PCBs though the boards were gold plated for better conduction.

2.6 Main Project stages

.

- Have new version 2 prototype boards professionally built, using best practice manufacturing techniques
- Test and evaluate the boards
- Research techniques that could be used to make improvements to the boards
- Implement design changes and have the new boards professionally manufactured
- Re-test and evaluate the new design and compare with the previous design

3.0 Testing

New versions of the V2 PCBs needed to be created; the bare boards were manufactured by the external contractor who had initially manufactured them as they had the necessary information to do so. The new V2 boards had the same layout as previously, however with the addition of gold plating the contacts on the board. A new manufacturing contractor which I had experience with was given the task of populating the components on the PCB using best practice techniques.

Once the V2 circuit boards had been manufactured and been populated with all components using best practice techniques it was ready for testing. At this stage of the project the national instruments equipment was not available, however an emulator board was available, which had been designed to control the switching of the units under test.

The emulator board was created by the project team in the early stages of the project and was used by them to test the switching of channels until they introduced the national instruments system. In conjunction with the emulator board a function generator was used to create the sinusoidal signal and an oscilloscope was used to monitor the resulting waveform.

3.1 Functionality

3.1.1 The test:

With the equipment set up, the functionality of the prototype then needed to be tested. Each electrode would need to be checked to ensure it could send and receive a signal. I did this by setting the prototype to send and receive a signal on the same electrode thus checking the signal could travel throughout the entire circuit as expected.

Fig 3.0 Shows a sample of the EIM main board circuitry. A constant current sine wave which is generated on the daughter board is switched through the ADG2128 device to the electrode. In its normal operation the system would then switch the signal read at a different electrode through the AD8114 device. However as I wish to check that each electrode can be selected both as a send and receive, for this test the send electrode is then switched through the AD8114 device to check the complete circuit.

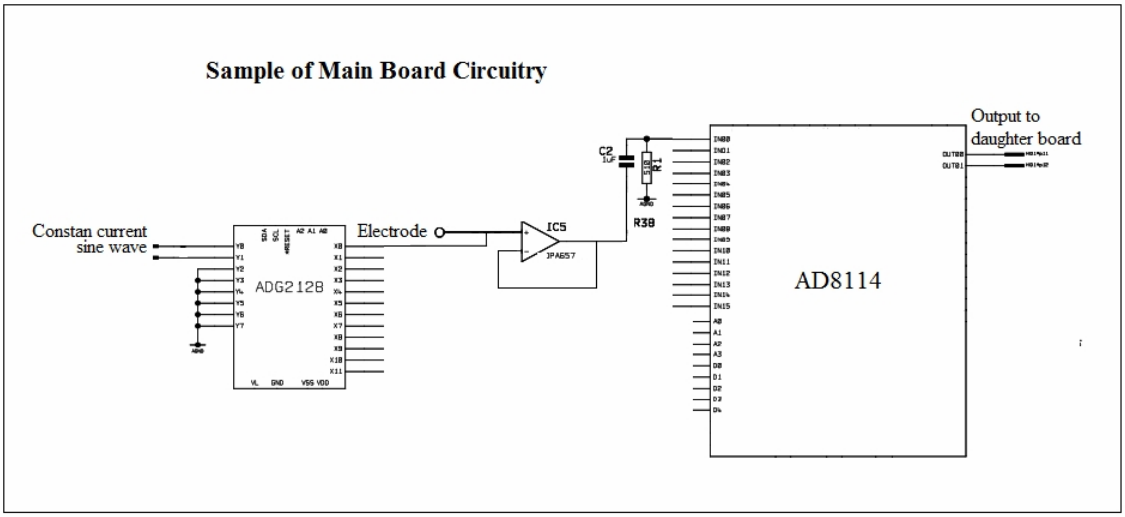

3.1.2 Results:

Immediately after powering up the board the power supply started to current limit and a couple of diodes failed. Testing was suspended whilst the cause of this problem was investigated. After some investigation a number of minor issues were discovered with the quality of the design and manufacture, once these were corrected functional testing continued.

Although the signals were very noisy all but five electrodes could have the signal switched through them. Of the five faults one signal was attenuated and four did not make it to the daughter board. The sinusoidal wave comes from the daughter board and goes to the ADG2128 devices on the main board, which are used to switch the signal to the correct electrodes. The outputs of these devices are then connected to the electrodes. This is the point at which the signal would enter the body. Each electrode is also able to receive signals. The electrodes are connected to an op amp which is used as a buffer and then the output of the buffer is connected to the input of the AD8114 switching devices which control which return signal it wants to look at and switches it through to the daughter board (see *Fig 3.0*).

Further investigation showed that one of the AD8114 devices had failed during the test and was not switching some of the channels through. During the test I observed that the AD8114 device was getting very hot which could explain why the device had failed. Before testing the performance of the V2 prototype the heating effect of the AD8114 devices needed to be evaluated to see if it was an issue.

4.0 Heat

The datasheet for the AD8114 device states that the operating temperature range is between –40°C and 85°C [64]. I devised a simple test whereby the temperature of the device was recorded over a time period of 40 minutes, to observe the temperature it reached. A thermocouple was covered in a heat conducting compound and attached to the top of the AD8114 device. Starting from the ambient room temperature in an air conditioned environment set at 24°C a temperature reading was taken at regular intervals from a calibrated digital thermometer. Firstly the device was tested with no signal passing through it and then it was left to cool and tested again with a signal switched through.

As can be seen in the results *table 4.0* and represented in *Fig 4.0*, with no signal switched through the device, the temperature of the device peaked at 71.2°C which is under the maximum running temperature, but it is still quite hot for a device in its quiescent state. What can also be seen in the table is that the results for the device, when a signal is switched thorough were stopped after 10 minutes. This was done because the temperature of the device had nearly reached the device's maximum operating temperature and was still rising. The test was stopped to avert yet more devices from failing.

4.1 Heat effect test results

Table 4.0 V2 AD8114 Heat Effect Results

Time in Mins	No signal	With signal
at ambient	25	26.5
0.5	32	46.6
1	37.5	53.2
2	45.2	62
3	49.7	67
4	52.7	71.8
5	55.1	74.6
6	57	76.4
7	58.9	78
8	59.7	79.3
9	61.2	80
10	61.8	81
11	62.8	Stopped
12	63.6	
13	65.5	
14	66.2	
15	67.6	
16	67.5	
17	68.4	
18	70.4	
19	70.1	
20	69.1	
21	69	
22	69.3	
23	69.4	
24	69.4	
25	69.2	
26	69.7	
27	70	
28	70.2	
29	70.3	
30	71.2	
31	70.9	
32	70.8	
33	70.7	
34	70.8	
35	70.8	
36	71	
37	71	
38	67.1	
39	67.5	
40	67.5	

Fig 4.0 AD8114 Heat Effect Results

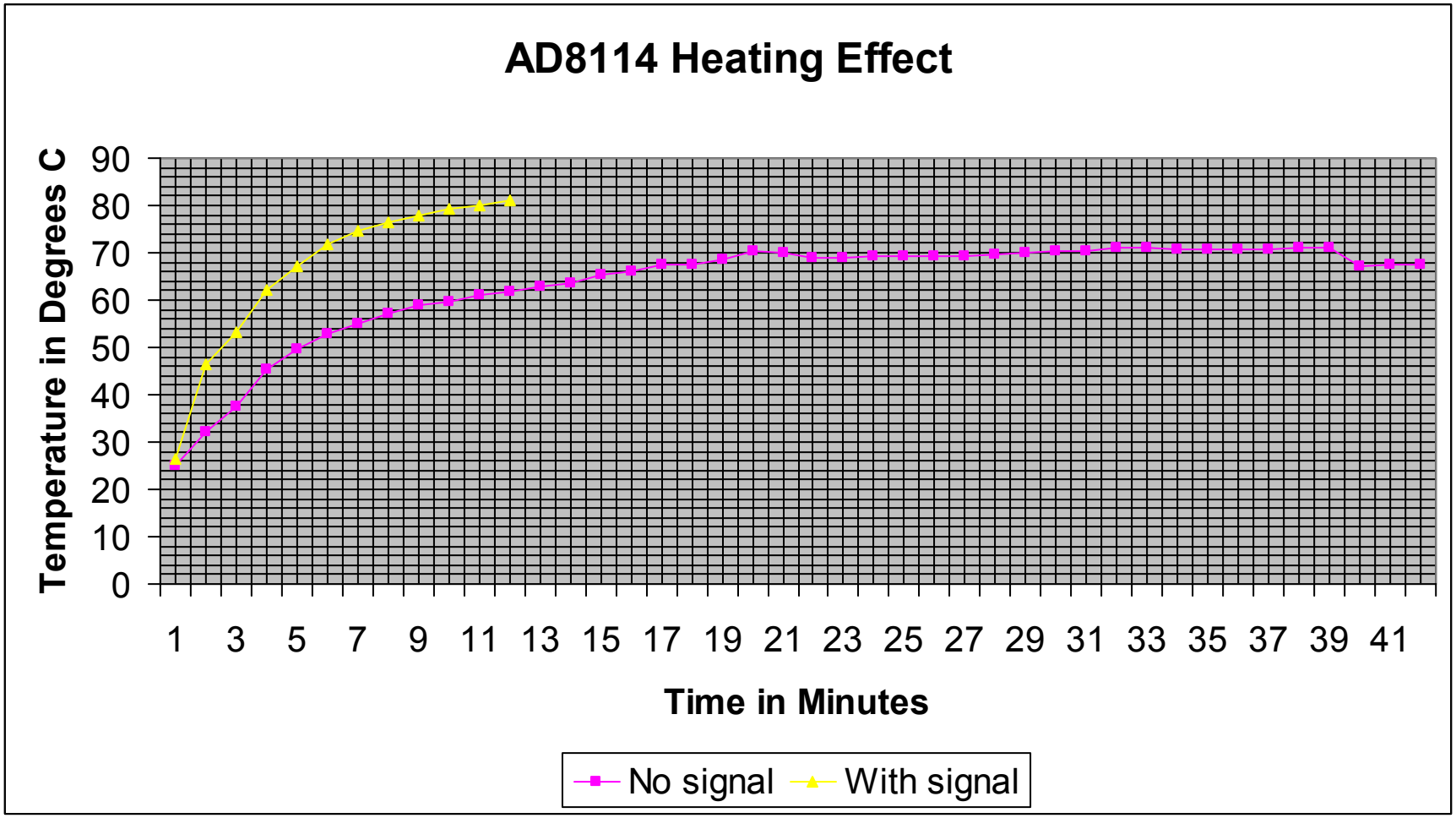

In the opposite side of the board directly under each of the AD8114's, an ADG2128 is situated, this also gets hot during testing and it was necessary to determine if this was the device overheating and causing the AD8114 to get hot or vice versa. There are also ADG2128 devices on the board which are not situated beneath the AD8114 devices, I devised a test where the temperature of the ADG2128 device was recorded under different circumstances. Firstly an ADG2128 device that is not under an AD8114 was tested without a signal being switched through and then again with a being signal switched through. Next an ADG2128 device that was situated beneath an AD8114 device was tested with no signal being switched through, and then with a signal switched through. These tests were done over a period of 10 minutes to prevent damage to the AD8114 device. The results of these tests can be seen in *table 4.1* and a graphical representation can be seen in *Fig 4.1.*

It is clear from the results of this test that the ADG2128 does not generate the heat of the AD8114. When an ADG2128 is separated from the AD8114 it clearly does not generate the same temperatures over the same time period as the AD8114 both in its quiescent state and with a signal switched through it. With the ADG2128 under the AD8114, the temperature it reaches both in its quiescent state and with a signal switched through are higher than the isolated device but clearly not in the temperature region of the AD8114. This indicated that it is the AD8114 generating the excessive heat, and not the ADG2128 devices, however ways of reducing the heating effects of the ADG2128s should be researched, and more importantly before doing any further tests on the board ways of reducing the heat produced by the AD8114 device needed to be investigated.

Table 4.1 ADG2128 Heating Effect

Time in Mins	Not under AD8114 no signal	Not under AD8114 with signal	Under AD8114 No signal	Under AD8114 with signal
Ambient	24.7	28	28.8	28.9
0.5	26	33.9	32.5	35.2
1	28.8	34.9	36.5	37.1
2	34.5	36	41.4	43.3
3	37.7	38.4	43.8	45.8
4	39.9	40.6	45.9	48
5	41.6	42.2	47.8	50.1
6	43.1	43.2	49.7	53.7
7	44.1	44.5	51.1	59.4
8	45	45.3	51.9	60.9
9	45.5	46.3	52.5	62.2
10	45.9	46.6	53.5	63.1

Fig 4.1 ADG2128 Heating Effect

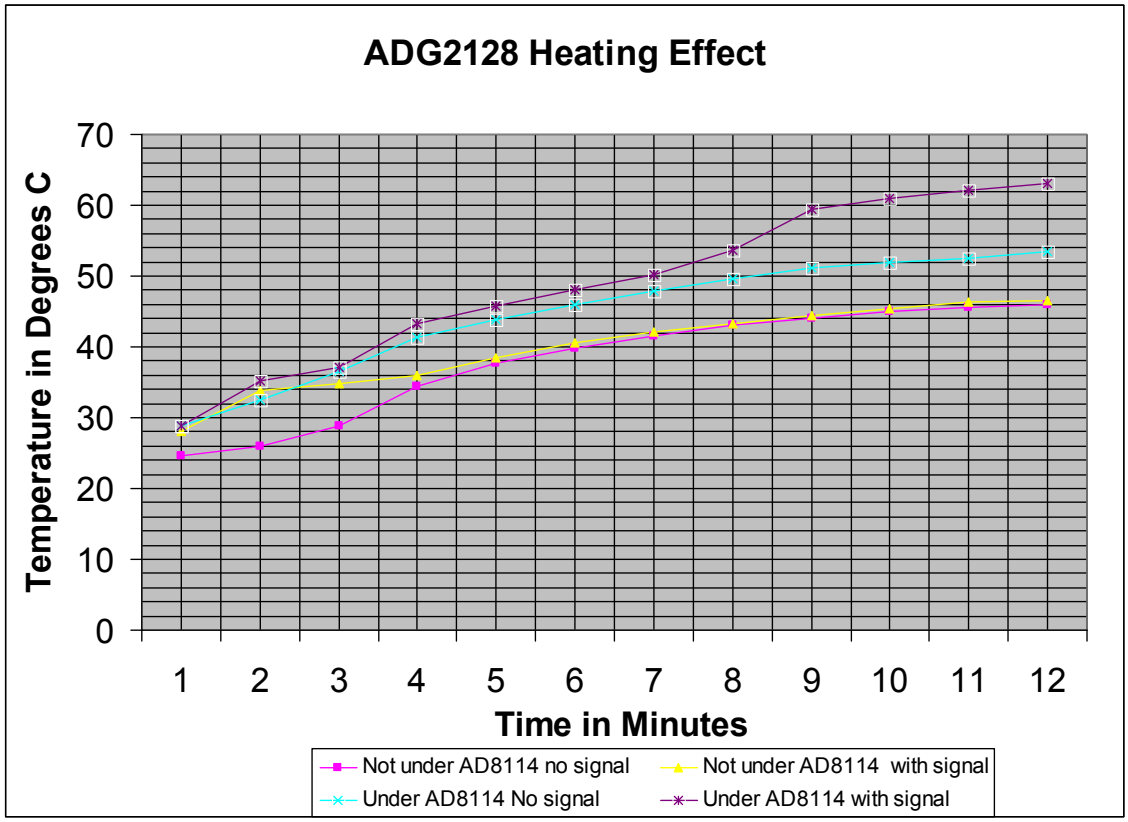

4.2 Heating Effect

Initially it was necessary to investigate how to stop the AD8114 from generating excessive heat. The datasheet for the AD8114 device stated "To control enable glitches, it is recommended that the disabled output voltage be maintained within its normal enabled voltage range (±3.3 V). If necessary, the disabled output can be kept from drifting out of range by applying an output load resistor to ground" [64].

As correcting the voltage supplies on the V2 prototype would take a great number of modifications, I decided to first add modifications to tie all unused inputs and outputs on the AD8114 to ground via a 1k resister. Then I carried out a test to see if this would significantly reduce the heating effect of the AD8114 devices. The test was carried out over the same time period as before and with the device in its quiescent state and with a signal switched through. These results were then compared with those carried out previously and the results can be seen in *Table 4.2* and are graphically represented in *Fig 4.2.*

What can be observed from these results is that the readings of the board in its quiescent state do not alter a great deal, whereas the readings taken of the device when a signal was being switched through were greatly improved, and this time it did not have to be switched off early due to overheating. Following from these new results I decided that any changes to the power supplies would be designed into the V3 prototype and not modified on the V2 prototype.

Table 4.2 Heating Effect between Modified and Un-modified V2 Boards

Time in Mins	no signal	With signal	Unused O/P to gnd via a 1K resistor no signal	Unused O/P to gnd via a 1K resistor With signal
at Ambient	25	26.5	30	30
0.5	32	46.6	33	45.8
1	37.5	53.2	37.6	52.7
2	45.2	62	45.3	57.8
3	49.7	67	49.7	62
4	52.7	71.8	52.7	65.2
5	55.1	74.6	55	67.5
6	57	76.4	56.9	69.1
7	58.9	78	58.9	70.1
8	59.7	79.3	59.6	71.3
9	61.2	80	61	71.6
10	61.8	81	61.6	72.3
11	62.8	Stopped	62.7	72.6
12	63.6		63.5	73
13	65.5		65.3	73.6
14	66.2		66	74.1
15	67.6		67.3	74.1
16	67.5		67.2	74.7
17	68.4		68	75.3
18	70.4		70.1	75.7
19	70.1		69.9	76.1
20	69.1		70	76.2
21	69		70.1	76.4
22	69.3		70	76.6
23	69.4		70	76.8
24	69.4		69.9	77.1
25	69.2		70	77.6
26	69.7		69.8	77.6
27	70		69.7	77.9
28	70.2		69.7	77.8
29	70.3		69.8	78
30	71.2		69.7	74.7
31	70.9		69.4	74.8
32	70.8		69.3	75
33	70.7		69.1	73.9
34	70.8		69	74.6
35	70.8		69	74.2
36	71		68.9	74.7
37	71		69	73.8
38	67.1		68.9	74.5
39	67.5		68.9	75.1
40	67.5		68.8	76

Fig 4.2 Heating Effect between Modified and Un-modified V2 Boards

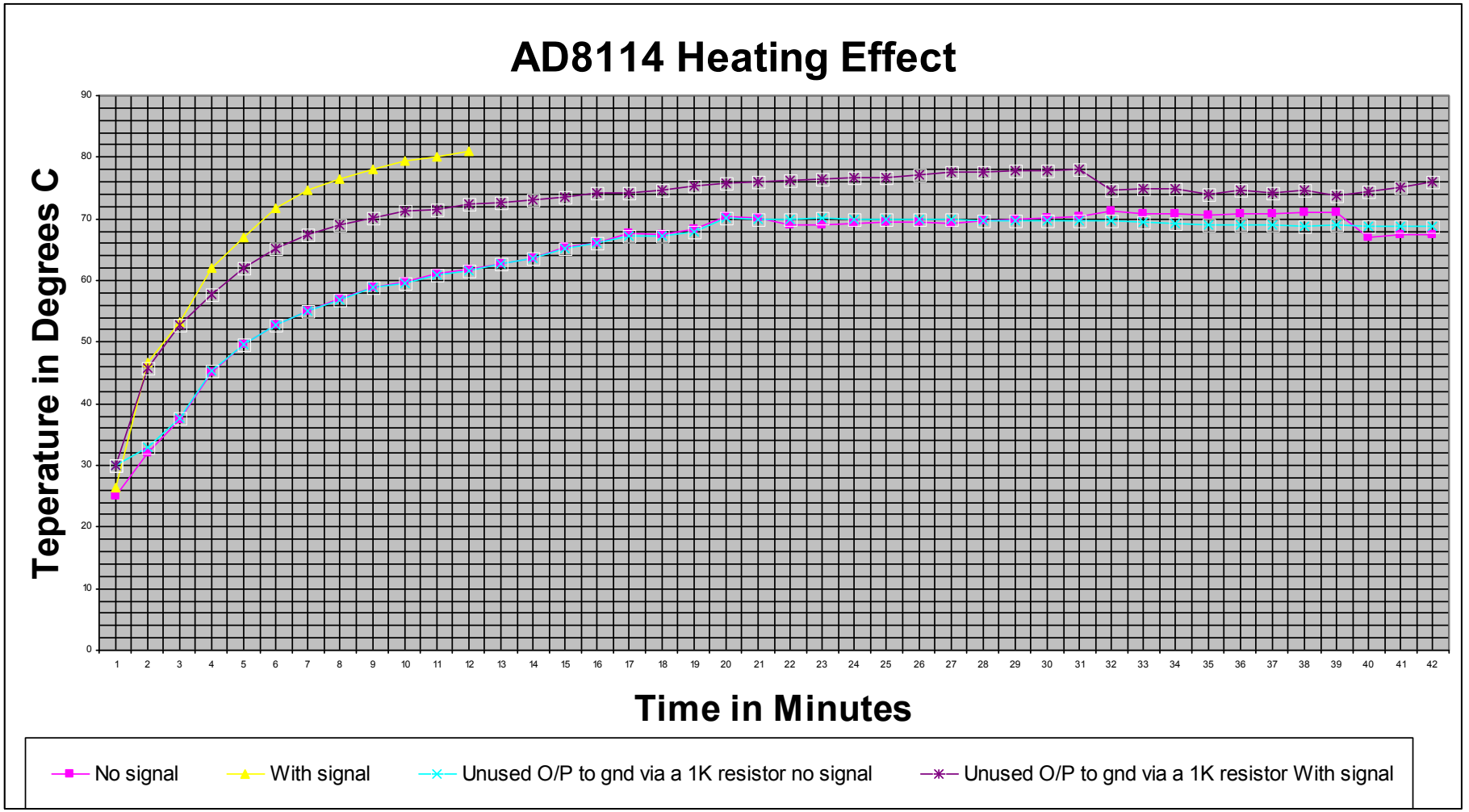

5.0 Noise

With EIM, fairly large changes in conductivity within the area being analysed will only generate comparatively small changes in voltage at the surface area. Small errors in the measured voltage, both random and systematic can cause large errors in the calculated approximation of the conductivity distribution during the image reconstruction process, thus limiting the resolution, accuracy, and sensitivity of the image [65].

It is therefore crucial to remove any unwanted signals from the system. During the functional test it was obvious there was excessive noise in the circuit, therefore I needed to carry out a test on the main and daughter board at different stages to see if there was any clear area that the noise was being introduced, in *Fig 5.0* the stages that were evaluated can be seen. The stages that were evaluated were:

- The input of the daughter board (TP1)
- The output of the VI stage (TP2)
- The input of the first switching device (TP3)
- The electrodes (TP4)
- The output of the buffer (TP5)
- The output of the second switching device (TP6)
- The input of the switching device on the daughter board (TP7)
- The output of the switching device on the daughter board (TP8)
- The differentiator on the daughter board (TP9)

Fig 5.0 Shows a sample of the daughter and main board circuitry Highlighted in red are the test points where the measurements were taken.

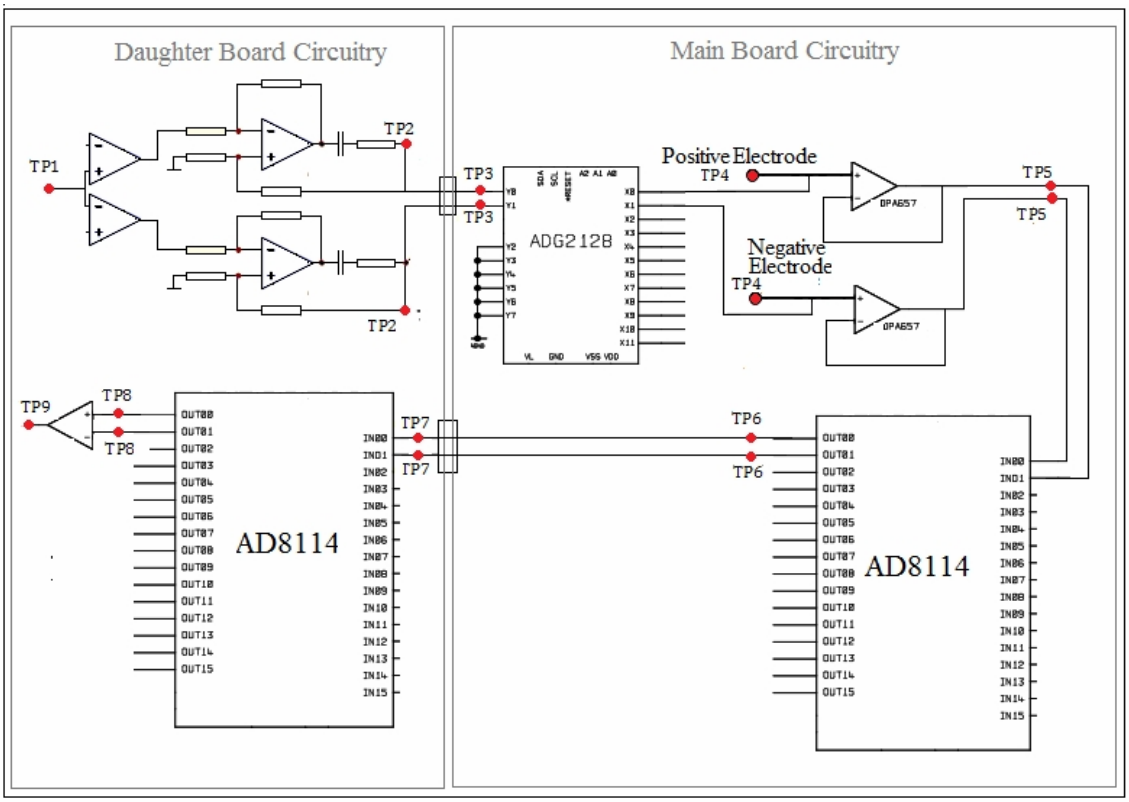

The test showed that large amounts of noise were introduced at the op amp buffers the results of which are in *Table 5.0* and the can be seen in *Table 5.1* which shows screen prints of the signal and noise level of the positive and negative input and output of the op-amp buffers. The top signal is the input signal to the daughter board; the bottom signal is the one that is being measured. The test results also showed large amounts of noise measured at the output of the differentiator device.

However this could be because the device has a minimum gain of 10 and was amplifying the noise that was already present in the circuit. Also as the electrodes are both acting as transmitters and receivers and therefore a much larger signal than would be generated under its intended use was being read back.

The output of the differentiator clips as its input signal is so high (1V) and because the differentiator device has a gain of 10 but only a +/- 5V supply. This means that the noise is amplified by gain of 10 but the signal can only go to a gain of 5 before clipping and the noise swamps the signal. For preliminary testing the differentiator output is ignored and the final signal readings where taken at the differentiator inputs.

Table 5.0 Readings taken from test points highlighting noise levels

Test point	NOISE Vrms	AMPLITUDE Vrms	SNR IN dB
+ Electrode	0.011	0.245	27.3
- Electrode	0.013	0.241	25.5
+ Op amp O/P	0.106	0.391	11.3
- Op amp O/P	0.078	0.371	13.6

Table 5.1 Noise levels at electrodes and op-amp buffers

Positive signal at electrode	Positive noise at electrode
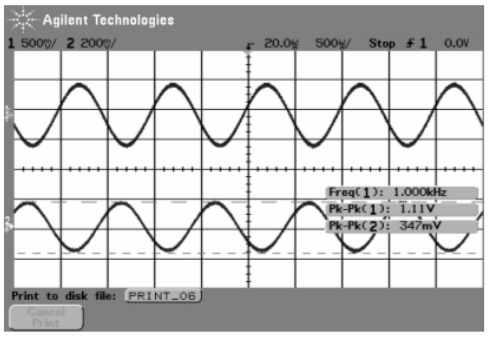	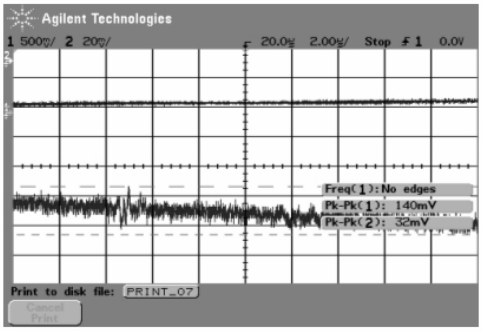
Negative signal at electrode	Negative noise at electrode
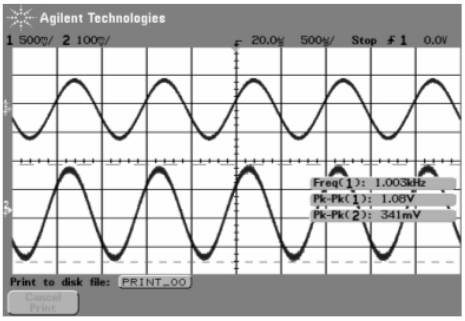	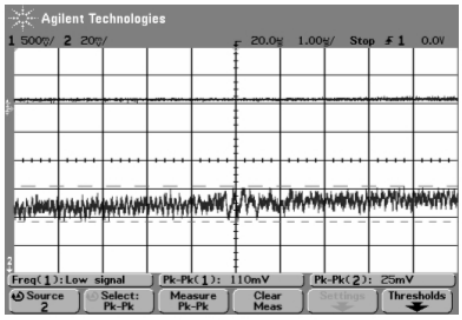
Positive signal at op amp output	Positive noise at op amp output
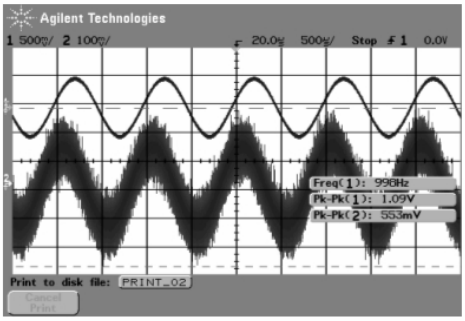	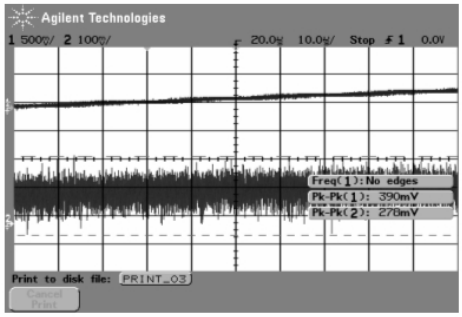
Negative signal at amp output	Negative noise at op amp output
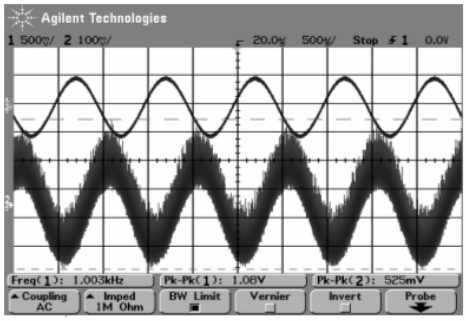	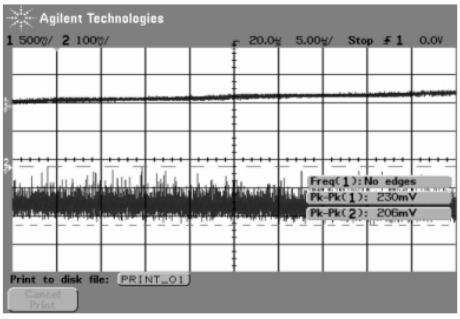

5.3 Possible causes of noise generation

Noise reduction techniques needed to be investigated and the board reviewed to see if any improvements could be made. Due to the fact there was so much noise in the later stages of the circuit, along with the limited equipment available at the time, it was hard to distinguish which types of noise were affecting the circuit. The noise issue is not specific to EIT, it can be generated in any analogue and digital circuitry as such an investigation of noise generally found in mixed analogue and digital circuitry was carried out. When implementing any design modifications intended to improve the noise level however, the improvements would need to fit the requirements of the EIM system.

5.3.1 Types of noise or interference

Internally generated:

- Thermal Noise
- Semiconductor noise (Shot noise)
- $1/f$ Noise
- Coupling (inductive, impedance and DC Power supply)

External Noise or Interference:

These are externally generated interfering signals or stray pick up which can be made up of:

- Mains Hum (50Hz) – This should not be an issue as the final system will be battery powered to aid in reducing noise.
- Radio Frequency coupling
- Switching spikes – especially when switching inductive loads

5.3.1.1 Thermal Noise:

Thermal noise which is sometimes referred to as Johnson noise [66] or Nyquist noise [67] is the random fluctuations in voltage created by the thermal agitation of electrons in a conductor [66]. The thermal noise level will usually vary in proportion with the temperature. This noise occurs over the entire spectrum and is independent of signal frequency. Cooling resistive and inductive components down will help to reduce thermal noise and it is possible reducing resistance in the circuit will reduce the thermal noise [68]. As seen in the previous temperature tests performed on the V2 prototype the multiplexers in the circuit generated the most heat. If the improvements made to the V3 prototype are successful the heat generated by these devices should be reduced and by doing so thermal noise should be proportionally reduced.

5.3.1.2 Semiconductor noise:

Semiconductor noise (Shot noise) initially discovered in 1918 by Walter Schottky [69] is similar to thermal noise except it is independent of temperature and is independent of signal frequency for a fixed bandwidth. Shot noise is created by random fluctuations of the electric current of a conductor and is often an issue crossing a potential barrier such as p-n junctions. [68][70][71]. I decided to perform an experiment to see if better performance can be obtained by replacing any semiconductor devices with alternatives to see if this could reduce this type of noise. The noise tests already performed on the V2 board highlighted the op-amps as the area which generated the largest amounts of noise so alternative op-amps should be evaluated to see if this will improve the noise levels.

5.3.1.3 1/f Noise:

1/*f* noise is generated when a dc current is applied where there is imperfect contact between two conducting materials causing the conductivity to fluctuate. It occurs in any device where two conductors are joined together. This type of noise is known as 1/*f (one-over-f noise*) noise because it increases at low frequencies, it is also referred to as low-frequency noise or flicker noise [70] as it is more prominent at lower frequencies a high pass filter should aid in its reduction.

5.3.1.4 DC Power supply coupling

Power supply coupling is the undesired coupling between subsystems via the power supply connections. The noise caused by power supply coupling can cause crosstalk in digital systems. Decoupling can be used to reduce this effect. Localised capacitors are connected close to the supplies of any IC's they act as a small, localised energy reservoir.

They take RF energy generated by rapid changes of current demand on the power supply during switching, and then convey it to the ground return path, preventing the voltage on the power supply rail from being pulled down by the momentary current load.

Consulting the datasheets for the AD8114, ADG2128 and OPA657 devices the AD8114 supplies should be decoupled with 0.1μF capacitors. The ADG2128 should be decoupled with 0.1μF in parallel with a 0.01μF capacitor and the OPA657 device should be decoupled with 0.1μF in parallel with 2.2μF capacitors. Examining the version 2 boards showed that these devices were not decoupled correctly. It appeared that the correct capacitor values were on the power rails but they were all round the outside of the board and nowhere near the devices that they were supposed to be decoupling [64] [72] [73].

5.3.1.5 Capacitive coupling

Capacitive coupling is unwanted capacitance between two PCB tracks or wires that are next to each other. Often one signal can capacitively couple with another where inputs can pick up a sympathetic signal from a track nearby. To reduce this capacitive coupling, tracks where this effect is likely to occur should be kept apart and where this does not suffice add screening in between these tracks with a ground plane. [74]. When examining the V2 board it was noted there are often signal tracks that run unnecessarily close to one another.

5.3.1.6 Inductive coupling

Inductive coupling occurs when currents flowing in conductors create magnetic fields that circulate around the currents. This then generates voltages in any other linked conductors. To avoid Inductive coupling from occurring it is best practice to avoid large areas in circuit paths and to try and avoid closing the circuit in a loop. The addition of a ground plane will also help to reduce this effect [64][75].

The version 2 board has been designed with both power lines and analogue and digital signal lines running around the board in a big loop. The project team had realised this was causing a big problem and had cut the tracks in the PCB to try and eradicate it, however there may still be a path through components and this could still be causing a problem.

5.3.1.7 Radio Frequency coupling

Radio frequency pick up e.g. mobile phones, radio and television signals etc can cause parts of the circuit to act as resonant circuits which can cause interference and noise. To help reduce this pick up use shielding, to try and avoid closing the circuit in a loop, keep leads short and use ferrite beads [74]. As mentioned under the heading “Inductive coupling” there could be a problem on the V2 main board with a circuit loop.

5.4 Noise and interference reduction techniques

5.4.1 Shielding

Critical areas of a circuit can be shielded by surrounding them with a conductive exterior. Electromagnetic fields in that occur near a shield will either be reflected or absorption by it as shielding provides a return path for filtered currents and protects against direct field coupling. [75]

5.4.2 Filtering

Filtering is a useful way of removing noise from a circuit. Low pass filters can be used to remove noise that occurs above a certain frequency and high pass filters can also be used to remove noise that fall below a certain frequency.

There are several different ways of creating filters. The version 2 prototype currently has RC low pass filters with a cut off frequency of 300Hz at the output of all op-amps, this will help remove frequencies $1/f$ noise and until the system is battery powered, mains hum. The national instruments system has bandwidth limiting of 20MHz to help reduce high frequency interference from the final reading. Whilst looking at filtering on the V2 prototype it was observed that the RC filter that precedes the differentiator had a cut off frequency of 15Hz. This was deemed far too low and replaced with a filter with a cut off frequency of 300Hz.

5.4.3 Power and Ground lines

Circuit boards with precision frequency analogue circuits should not share the same grounds as digital circuits; this is because the digital ground noise may affect the efficacy of the analogue circuits. Ground paths for the analogue and digital circuits should be separated to avoid common impedance coupling [76]. Examining the V2 boards showed that the analogue and digital circuits ground had been commoned together.

Consulting the data sheet for the AD8114 and ADG2128 devices it was very clear that a lot of the design rules were not being followed when laying out the V2 board. The first major issue was with the power supplied to the boards. The supplies on the board are marked up as +5V analogue, -5V analogue, +5V digital and -5V digital.

It was unclear as to why there would be a -5V digital as the digital supply is only ever positive. The devices require the digital 5V supply to be separated from the analogue +/- 5V supply. The V2 prototype was then examined to see what each power rail was supplying. It became clear that best practice had not been followed, instead of separating the analogue and digital supplies for each device the AD8114 and ADG2128 had their supplies separated.

The ADG2128 was supplied with the rails marked digital +/- 5V and the AD8114 and the op-amps were supplied with +/- analogue 5V. Both devices require a digital 5V supply that are used to control switching and analogue +/- 5V, which are used to balance the signal (see *Fig 5.1*). Having only one supply source for each device and joining the analogue and digital supplies could have been inducing noise. The ADG2128 board has a pad underneath it which is supposed to be connected to a –5V supply. This was not being done and was compounded further as via holes were tracked under the device on the board, which the pad beneath the board could pick signals up from.

5.4.4 Board layout

The datasheet for the AD8114 device suggests a 4 layered PCB for use with the device. The data sheet states “unused regions of the four layers are filled up with ground planes. As a result, the input and output traces, in addition to having controlled impedances, are well shielded” [64]. This example was a good starting point but further investigation was needed into the best PCB layout for our requirements

Fig 5.1 Shows the difference between the power rails on the V2 switching circuits and the V3 switching circuits. The V2 does not separate the power rails as the device data sheets recommend whereas the V3 circuit follows the recommendations of the datasheets.

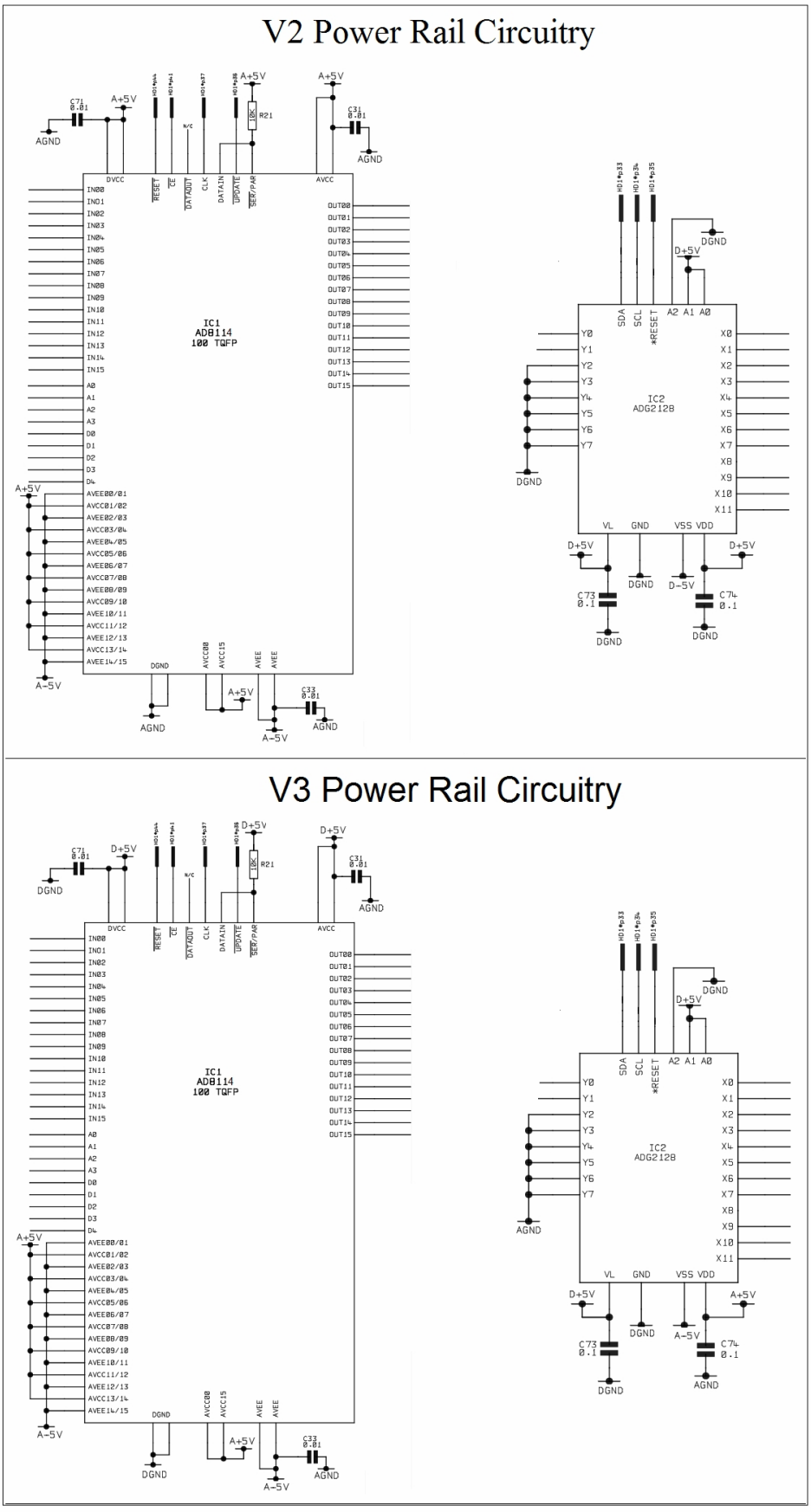

.5.4.4.1 Ground plane

A ground plane acts as a common reference voltage and can provide shielding. A ground plane can also enable heat dissipation and reduces stay impedance by magnetic field cancellation. Ideally a ground plane should be unbroken and dedicated as an entire layer of the PCB [75][76].

Having a large ground area adds distributed capacitance to all circuit components, which aids in suppressing radiated noise. It is necessary to keep analogue and digital grounds separate on the PCB and only connected at the power source [76].

5.4.4.2 Power planes

There are several reasons why having power planes on a PCB is preferable to having just tacked power lines. One possible problem with the V2 main board is a loop area in the circuit.

Power planes could help remove this problem as when return signals are on a plane immediately under a track, loop area is minimised. Power planes can also reduce crosstalk as it separates tracks and it can bring tracks and their reference planes closer together [77].

5.4.4.3 Tracking

- Avoid running lengthy parallel tracks in close vicinity to each other to reduce the chances of inductive coupling
- Avoid lengthy tracks on neighbouring layers to reduce capacitive coupling
- If possible signal tracks requiring high isolation should be tracked on separate layers. If this is not possible they should be tracked with a grounding surrounding them

When a track needs to change direction it is best practice not to use a 90˚ angle but to change direction in stages *Fig 5.2.* This is because at sharp angles signal reflection can occur. It is also better for the etching process as the acid can eat away at the corners and in thin tracks can cause problems [78][76].

Fig 5.2 Shows an example of best practice tracking having 2 45 degree angles instead of a 90 degree angle reduces signal reflection.

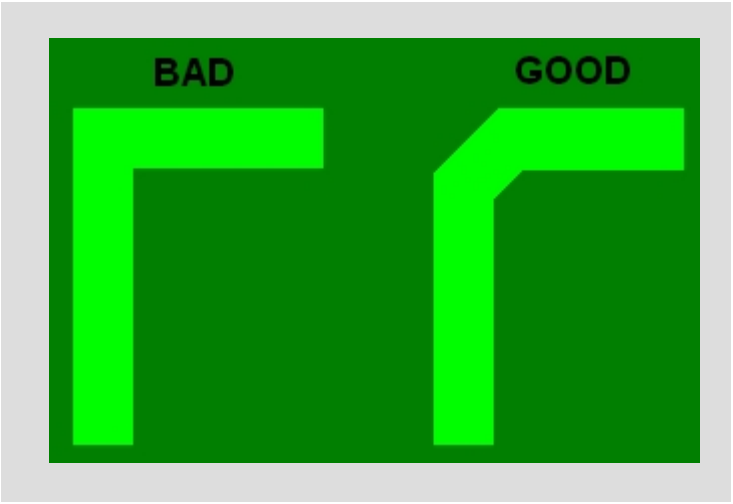

5.5 Op-Amp Testing

After consulting the data sheet for op-amps and examining the board it was clear that the devices were not being decoupled properly. I added modifications to a sample of the op amps, which included adding a 0.1μF and 2.2μF capacitors in parallel to the positive and negative voltage rails, however this did not make any significant difference to the noise level. The next course of action was to try different models and manufacturers of op-amps to see if the noise levels could be reduced. The op amps that were being used were OPA657's manufactured by BB.

I tried several different makes and models of op-amps with a wide bandwidth and fast slew rate replacing the OPA657's on the main board (OPA657 were also used in the VI stage of the daughter board but did not seem to produce the same symptom). The op-amps were then tested as part of the system, at 1kHz with a 1V PK-PK sinusoidal signal to see if any could improve on the signal produced by the OPA657. The readings were taken at the positive input to the differentiator (see *Fig 5.3*). The op-amps chosen for the test were:

- OPA657
- OPA656
- OPA820
- LM6714
- LINEAR 6205
- LMH6702
- LMH6645
- LMV796

Fig 5.3 Shows a sample of the EIM circuitry under test with the test point where the measurements are taken highlighted in red and the op-amp being tested circled in red.

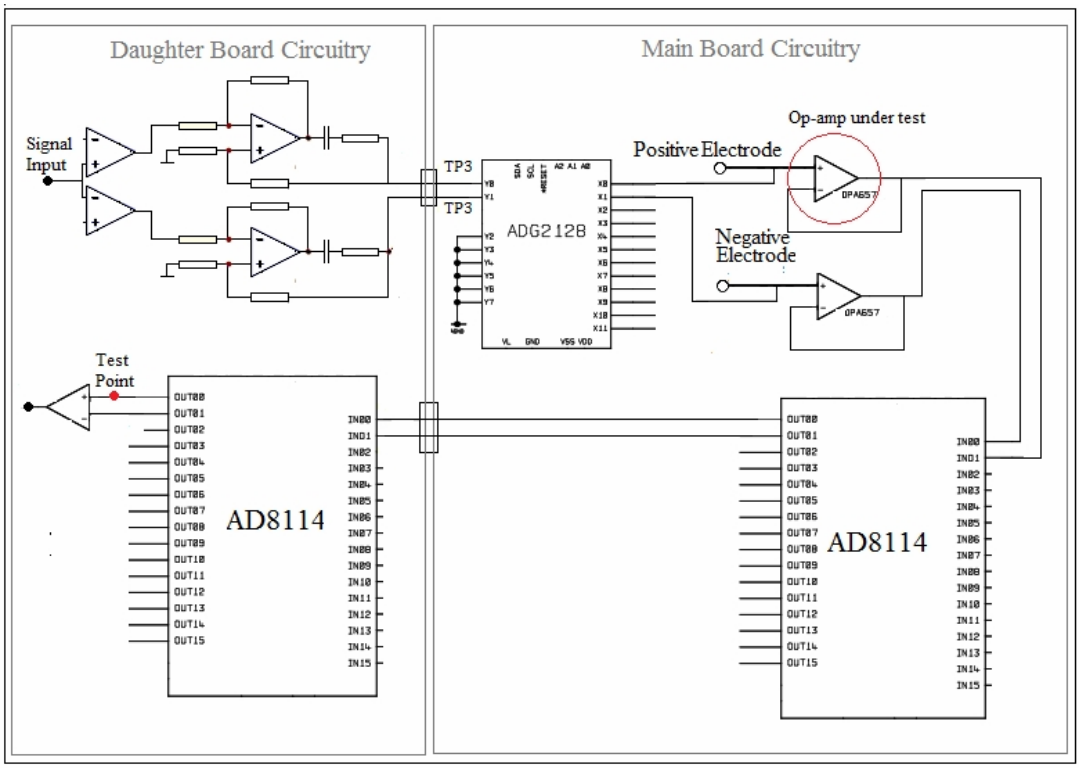

The results from these tests can be seen in *Table 5.1* and graphically represented in *Fig 5.4.* The signal to noise ratio was calculated using the formula $20*\text{Log10}(V_{rms} / \text{Noise}_{rms})$.

Table 5.1 Op-amp SNR test results

OP-AMP	NOISE	AMPLITUDE	SNR
LINEAR 6205	0.02	0.588	29.367
LMH6645	0.035	0.613	24.868
LMV796	0.021	0.3	23.098
LM6714	0.106	0.706	16.47
LMH6702	0.081	0.488	15.599
OPA656	0.125	0.706	15.038
OPA657	0.25	0.637	8.124
OPA820	0.519	1.01	5.7831

Fig 5.4 Op-amp SNR test results

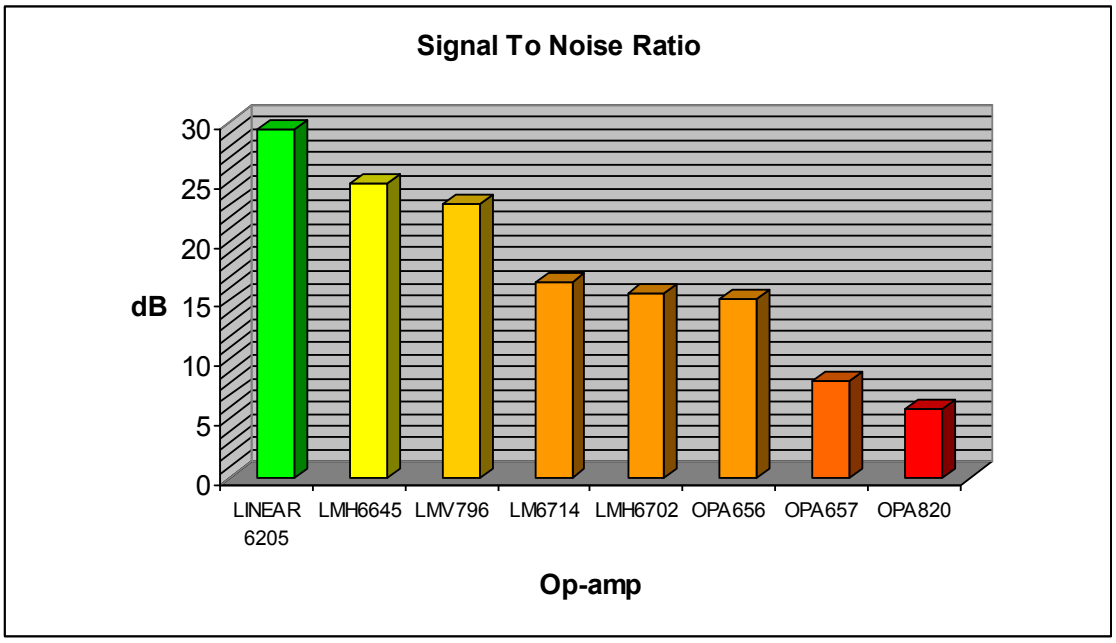

Out of the op-amps tested the LT6205 appears to have the best signal to noise ratio at 1kHz (green bar on *Fig 5.4*). The full scan of the system would be done over a range of frequencies from 1kHz to 10MHz. The higher the frequency the deeper the signal will penetrate into the body. The results from each frequency range are used to build up an image.

Each frequency represents a different level of the final image each level is an image of a different depth, these levels are added together to make a 3D representation. The op-amps therefore needed to be tested over the frequency range to find the op-amp that will work best over the whole frequency range.

This test was done using the following op-amps:

- OPA657
- OPA656
- LINEAR 6205
- LMH6702
- LMH6645

The LMV796 was not tested further as it attenuated the signal too much and the OPA820 SNR was too low. The OPA656 was kept as the project team had asked for this specific op amp to be tested. The op-amps were tested at 1kHz, 1MHz and 10MHz. This produced the results seen in *Table 5.2, Table 5.3* and *Table 5.4*.

Table 5.2 1kHz Op-amp SNR Test

1kHz			
OP-AMP	**NOISE in Volts**	**AMPLITUDE in Volts**	**SNR in dB**
LINEAR 6205	0.02	0.588	29.36694661
LMH6645	0.035	0.613	24.8678486
LMH6702	0.081	0.488	15.59869606
OPA656	0.125	0.706	15.03789376
OPA657	0.25	0.637	8.123988473

Table 5.3 1MHz Op-amp SNR Test

1MHz			
OP-AMP	**NOISE in Volts**	**AMPLITUDE in Volts**	**SNR in dB**
LINEAR 6205	0.08	0.713	18.99999086
LMH6645	0.097	0.7	17.16652611
LMH6702	0.222	0.631	9.073527696
OPA656	0.294	0.775	8.419087442
OPA657	0.403	0.925	7.216733732

Table 5.4 10kHz Op-amp SNR Test

10MHz			
OP-AMP	**NOISE in Volts**	**AMPLITUDE in Volts**	**SNR in dB**
LINEAR 6205	0.3	0.328	0.77505178
OPA656	0.322	0.344	0.574051418
LMH6645	0.313	0.331	0.485673125
LMH6702	0.338	0.35	0.303026881
OPA657	0.463	0.416	-0.92975321

The results of these three sets of tests show the Linear LT6205 to be the best over the frequency range and comparable in price to the OPA657's, therefore the OPA657's that were fitted to the VI stage on the daughter board were replaced with the LT6205's. These op amps are depicted in *Fig 5.5*. At this point the National Instruments equipment became available, as this is the equipment that will run the final system I would use this equipment for testing from this point onwards.

Fig 5.5 Sample of the daughter board circuitry and the op amps which were updated

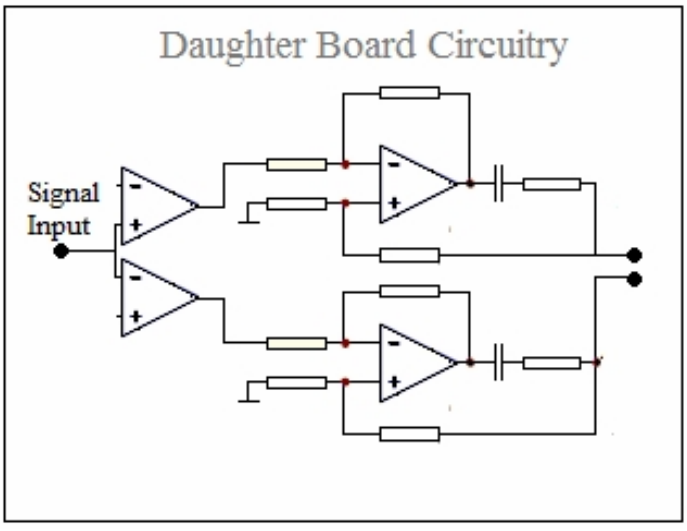

With the op-amps on the daughter board replaced the previous test needed to be repeated to see if there is any improvement. The same op–amps as before were used with the addition of the LT1880CS5 and LTC2054CS, as these two op-amps are by the same manufacturer as the LT6205 they were therefore tested for comparison purposes. In one case I replaced the buffer (see *fig 5.3*, ringed op-amp) by a direct link to determine what the base level noise would be without a buffer to give a baseline reading, however a buffer is required in the circuit to ensure the AD8114 device is not loaded. The results of these tests can be seen in *Table 5.5.*

The National instruments equipment has a lower bandwidth limiting than the oscilloscope, which may also improve the signal that is being read back. The program for controlling the national instruments equipment allowed the frequency to be adjusted between 1kHz and 10MHz but at the time did not allow for an adjustment in the amplitude which was set to 2VPK-PK

Table 5.5 1kHz Op-amp SNR test with NI equipment

AT 1kHz			
OP-AMP	**NOISE in Volts**	**AMPLITUDE in Volts**	**SNR in dB**
LTC2054CS	0.0009	0.55	55.72
LT1880CS5	0.001	0.55	54.80
Link	0.001	0.35	50.88
LINEAR 6205	0.005	0.55	40.82
LMH6645	0.007	0.55	37.90
OPA656	0.01	0.55	34.80
OPA657	0.03	0.55	25.26
LMH6702	0.03	0.55	25.26

It is clear from this experiment that at 1kHz the LTC2054CS gives the best result. These op-amps then needed to be tested at the other end of the scale to see if they can handle the higher frequencies, at the time I was unable to test the noise level effectively with the national instruments equipment so the sinusoidal wave was scrutinised visually. The results from these tests can be seen in *Table 5.6* and the screen prints of the tests can be seen in *Fig 5.6*, *Fig 5.7* and *Fig 5.8*

Table 5.6 1MHz op-amp SNR test with NI equipment

10MHz		
OP-AMP	**AMPLITUDE**	**QUALITY**
LINEAR 6205	20mV	Clean signal
LT1880CS5	5mV	noisy
LTC2054CS	4mV	noisy

Fig 5.6 LINEAR 6205

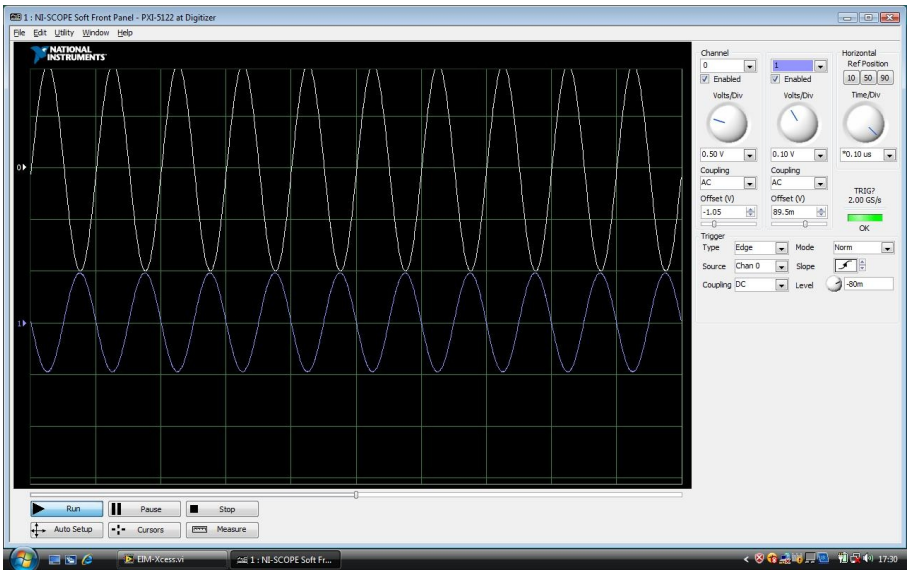

Fig 5.7 LT1880CS5

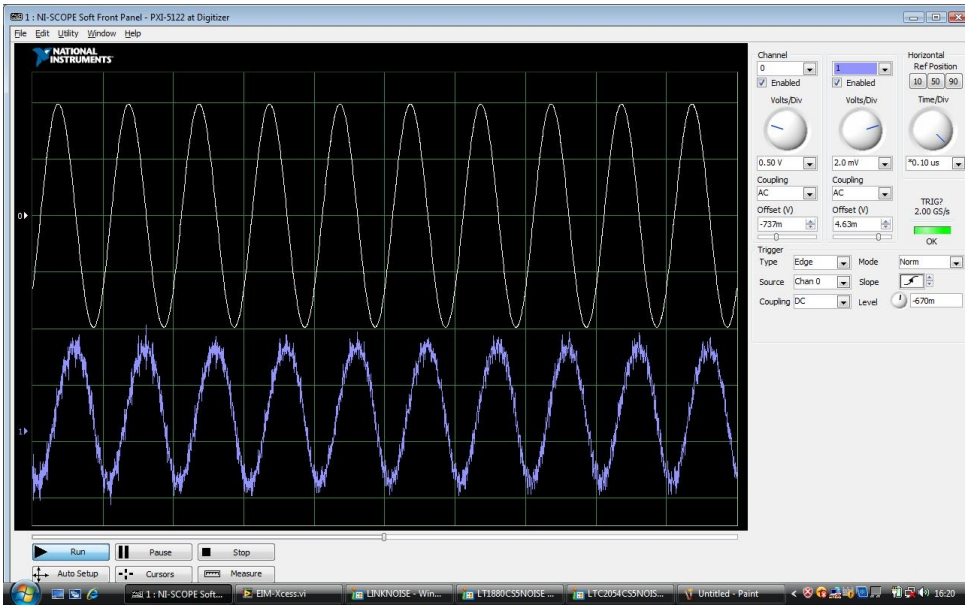

Fig 5.8 LTC2054

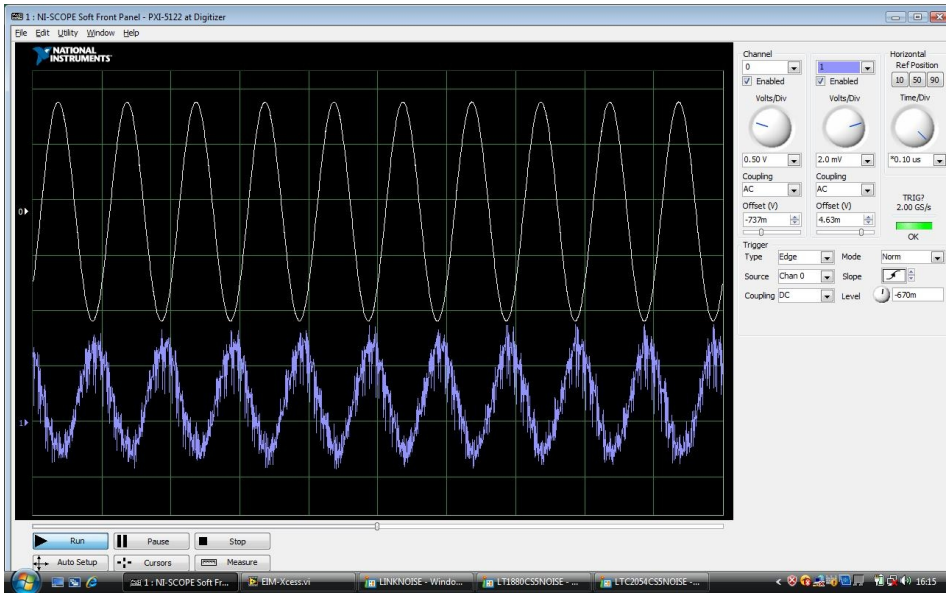

As can be seen from *Fig 5.6, Fig 5.7* and *Fig 5.8* it is clear that the LT1880CS5 and LTC2054 are not good enough at the higher frequency. Therefore I decided to use the LT6205 to replace the OPA657's at this point.

6.0 V3 Design

Using noise reduction techniques from research and the results of the investigation into heat reduction and op-amps, a new PCB layout was created from my specifications with the aid of manufacturing company's draughtsman. The changes made from these specifications on the V2 main and daughter boards to the V3 main and daughter boards were:

- The version 3 boards were changed from the version 2's, two layer boards to multi-layer boards with separate ground, power, analogue signal and digital signal layers. These can be seen in *Fig 6.0.* The ground and power planes will help dissipate the heat produced by the ADG8114 devices. Having power planes instead of tracks around the board will also help reduce the chances of magnetic fields from being created. Also having analogue and digital signals on separate layers helps reduce crosstalk.

Fig 6.0 New Board Layers

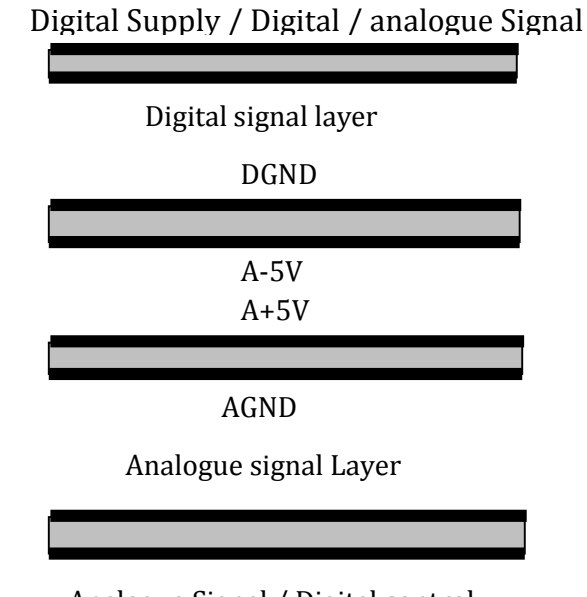

- Ground infill is used to fill any unused area of the PCB and between signal tracks. Filling the unused areas of the PCB with ground infill will act as a shield, which will reduce the effect of external RF interference. Having ground track in-between the signal tracks will help remove capacitive coupling

- Signal tracks were separated as much as possible to help avoid inductive coupling

- Decoupling caps (specified in the device's datasheets) are situated as close to the supplies of the devices to avoid DC power supply coupling

- All unused inputs and outputs are tied to ground via a 1K resistor as stated in the datasheet. As seen in the heat investigation this helps reduce the heating effect of the AD8114

The Gerber files of all these changes can be found in the Appendix

7.0 Evaluation of version 3 Prototype

Once the design changer to the version 3 had been completed which involved the schematic changes to the circuit design as seen in *Fig 5.1* and the layer and layout changes discussed in the previous chapter. PCB's were produced and they were populated with components using the same processes as the version 2 boards. The boards then had to be functionally tested.

7.1 Functional test

The functional test was the same functional test as performed on the version 2 boards whereby each channel is switched through on itself to check each channel is working. When testing the functionality of the version 3 prototype there were a few issues discovered, all of which were in the main board.

Firstly several channels were not switching a signal through; this was discovered to be caused by an error, made when laying out the PCB at the drafting stage. One of the ADG2128 devices had its chip ID tracked incorrectly which meant it had the same ID as another chip on the board and therefore switched channels through at the wrong time.

Cutting the incorrect tracks and using mod wire to connect the device to the correct tracks repaired this fault. Once this issue had been overcome there was also a further issue where on a few channels the signal was being attenuated. This transpired to incorrect value resistors being fitted as terminating resistors.

This was corrected on the board and both issues were corrected in the documentation for the boards. Once both these issues had been overcome the board functioned as expected. The next step was to test its performance.

7.2 Re-evaluate the heating effect

The next step was to perform the same temperature experiment on the V3 prototype as was previously performed on the V2. I carried the experiment out under the same conditions as before.

As can be seen in the results *table 7.0* and represented in *Fig 7.0*, with no signal switched through the AD8114 device on the V3 prototype the temperature of the device peaked at 43.8°C compared with 71.2°C on the V2 prototype. Originally on the V2 board when a signal was passed through the AD8114 device the temperature rose close to the maximum operating temperature of the device (85°C) within 10 minutes and the experiment had to be stopped. When testing the heating effect of the device on the V3 prototype the temperature peaked at 51.8°C. This is a much more acceptable operating temperature.

Table 7.0 Re-evaluation of the AD8114 Heating Effect

Time	V2 with no signal	V2 with signal	V3 no signal	V3 with signal
0	25	26.5	25.2	26
0.5	32	46.6	26	35
1	37.5	53.2	27.6	38.2
2	45.2	62	29.8	41.2
3	49.7	67	31.8	42.4
4	52.7	71.8	33.4	43.6
5	55.1	74.6	34.4	44.4
6	57	76.4	35.8	45.6
7	58.9	78	37.4	47
8	59.7	79.3	37.6	47.2
9	61.2	80	38	47.6
10	61.8	81	38.8	48
11	62.8	Stopped	39.4	48.2
12	63.6		39.6	48.6
13	65.5		40	48.6
14	66.2		40.2	48.8
15	67.6		40.2	49
16	67.5		40.6	49.2
17	68.4		41	49.6
18	70.4		41.4	49.6
19	70.1		41.4	49.8
20	69.1		41.8	50
21	69		41.6	50.2
22	69.3		42	50.6
23	69.4		42.4	50.6
24	69.4		42.6	50.8
25	69.2		43.2	51
26	69.7		43.2	51.2
27	70		43.8	51.6
28	70.2		43.2	51.8
29	70.3		43.2	51.8
30	71.2		43.6	51.6
31	70.9		42.6	51.4
32	70.8		43.4	51.2
33	70.7		43	51.4
34	70.8		42.6	51
35	70.8		42.2	50.8
36	71		42.8	51
37	71		43	51
38	67.1		43.2	51.2
39	67.5		43	51
40	67.5		43	50.8

Fig 7.0 Re-evaluation of the AD8114 Heating Effect

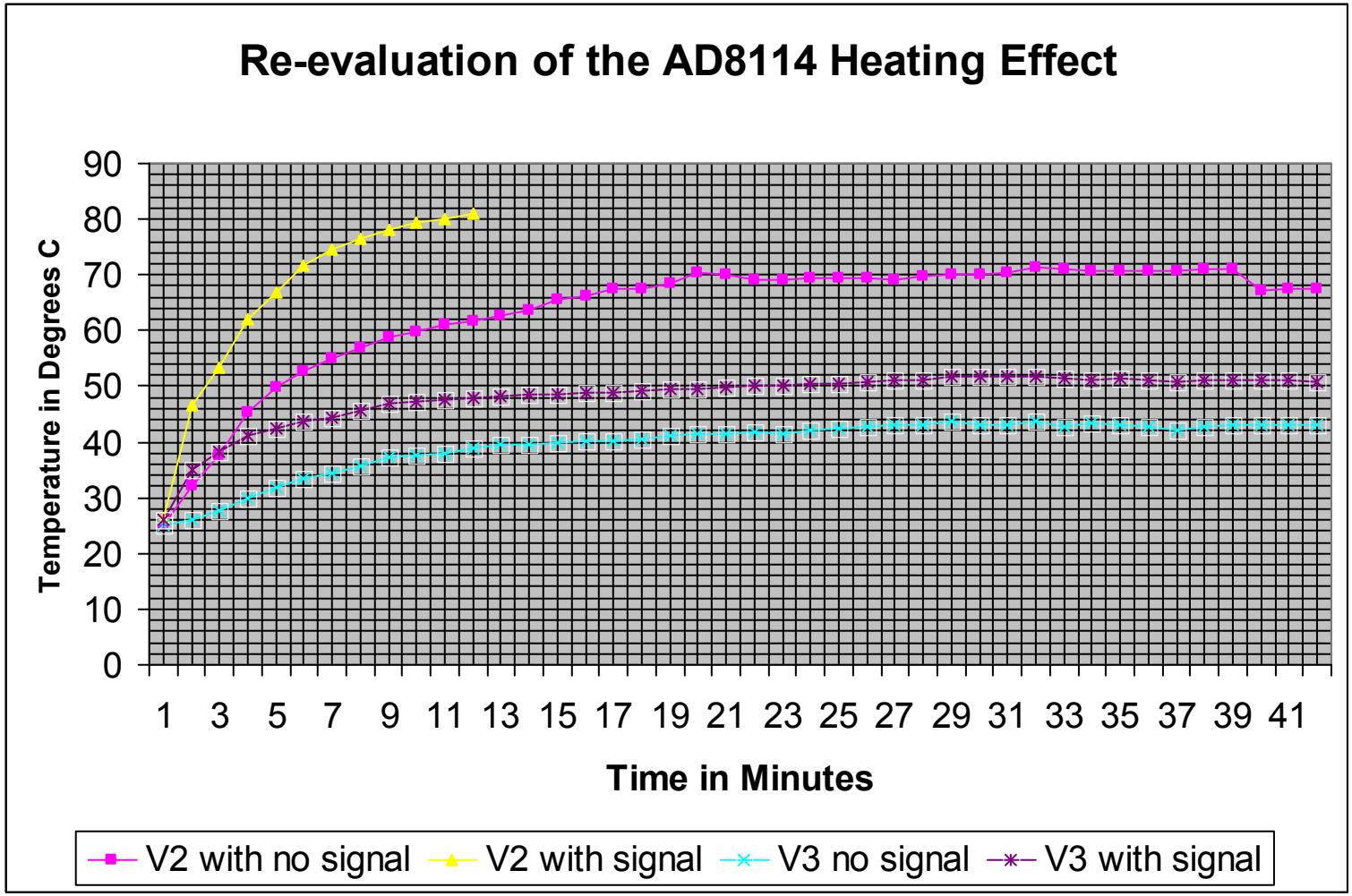

7.3 Signal test

The quality of the measured signals needed to be examined to see if they met the target of 60dB that had been set. Firstly the amplitude was measured and compared over the set frequency range. These results were then compared with the version 2 prototype, which had the modification gleaned from the noise reduction investigation performed upon it. The second step was to examine the noise levels present on the board. Finally the signal to noise ratio was calculated from these results.

7.3.1 Amplitude

For this experiment a sinusoidal signal over a range of frequencies was injected at the input stage of the daughter board. The main board will be set to send and receive the signal from the same electrode as for the + and – signals, eliminating any external influences from affecting the readings at this part of the circuit.

The signal was then read at several stages throughout the circuit, measuring the signal amplitude. The signal will be read at the output of the VI stage (TP1), the output of the main board AD8114 (TP2), the input to the daughter board differential amplifier (TP3) and finally the output of the differential amplifier (TP4). This is depicted in *Fig 7.1.*.

Fig 7.1 Shows a sample of the EIM circuitry under test with the test point where the measurements are taken highlighted in red.

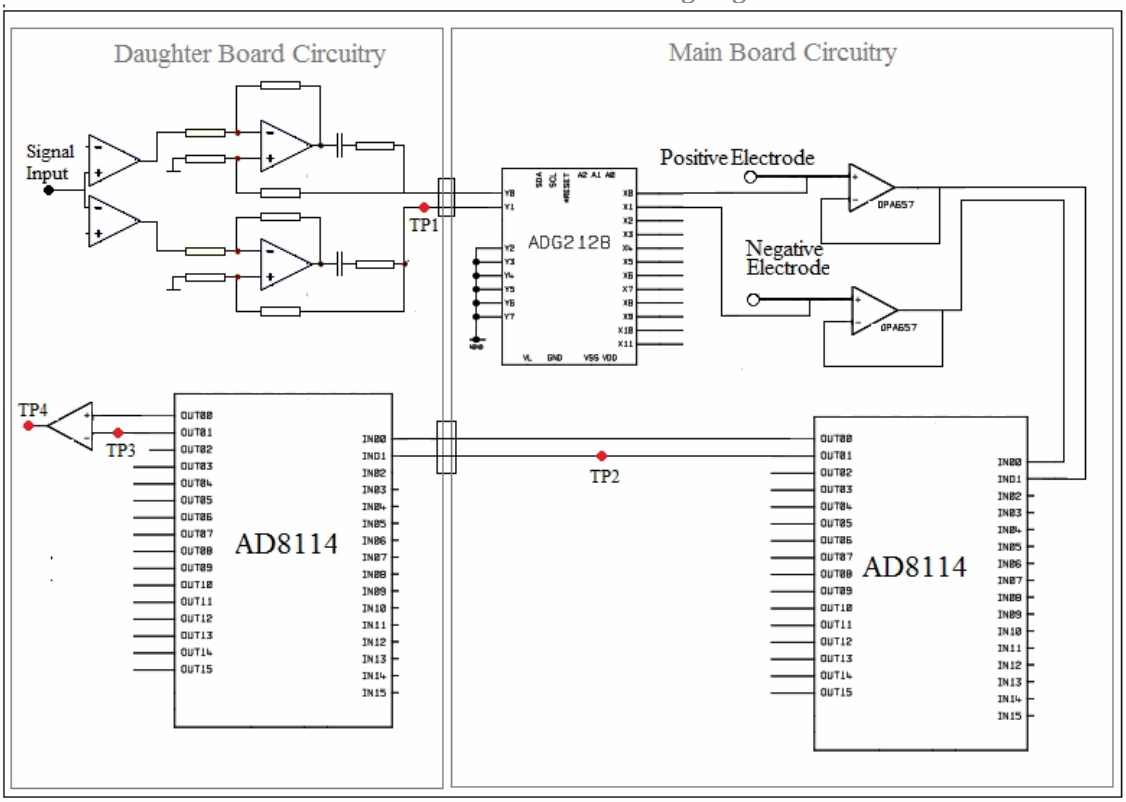

For the output of the VI stage, the output of the main board AD8114 and the input to the daughter board differential amplifier, the amplitude of the injected signal will be 2V PK to PK. For the differential output reading the signal injected into the daughter board input stage will be reduced to 250mV PK to PK as this device has a minimum gain of 10 and if its input is higher the signal starts to clip.

The lower input voltage will simulate the kind of signal the differentiator would get under when the electrodes are immersed in saline. To reduce the amount of readings needed, the readings were only being taken on the negative side of the circuit, apart from the differentiated output, which incorporates both positive and negative signals. Version 2 results can be seen in *Table 7.1* and are represented graphically in *Fig 7.2.* Version 3 results can be seen in *Table 7.2* and are represented graphically in *Fig 7.3.*

Table 7.1 Version 2 Results

Version 2				
Frequency	**Amplitude**			
	VI O/P	**Main board AD8114 O/P**	**Daughter board Diff I/P**	**Daughter board Diff O/P**
1kHz	0.623	0.552	0.56	0.98
5kHz	0.633	0.629	0.634	1.18
10kHz	0.634	0.633	0.637	1.193
50kHz	0.634	0.634	0.64	1.179
100kHz	0.634	0.638	0.644	1.183
500kHz	0.618	0.633	0.639	1.184
1MHz	0.558	0.607	0.609	1.137
5MHz	0.203	0.33	0.349	0.681
10MHz	0.86	0.137	0.144	0.326

Fig 7.2 Shows the version 2 amplitude response to frequency. The amplitude appears to be consistent until between 500 KHz and 1 MHz when it appears to tail off. The Differential is higher as it has added gain

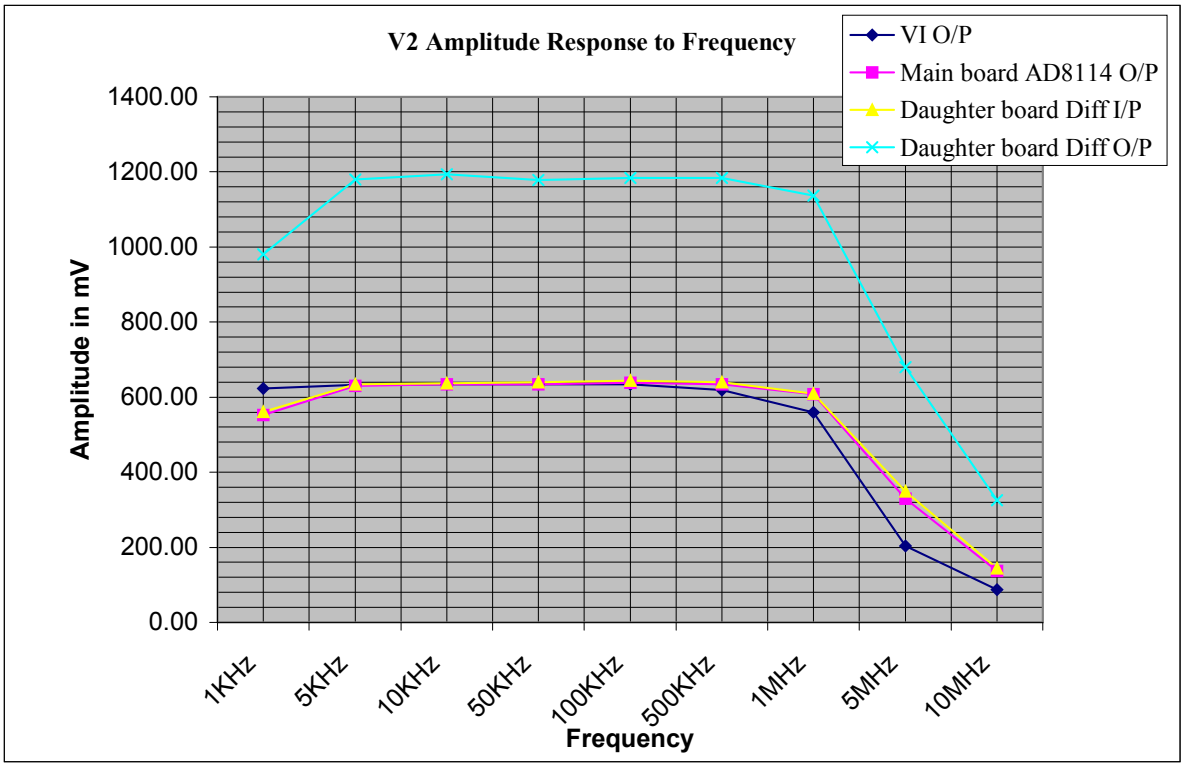

Table 7.2 Version 3 Results

Version 3				
Frequency	**Amplitude**			
	VI O/P	**Main board AD8114 O/P**	**Daughter board Diff I/P**	**Daughter board Diff O/P**
1kHz	0.61	0.546	0.549	1.627
5kHz	0.623	0.619	0.621	2.005
10kHz	0.623	0.624	0.623	2.067
50kHz	0.625	0.624	0.624	1.946
100kHz	0.627	0.629	0.629	2.013
500kHz	0.618	0.629	0.63	2.014
1MHz	0.518	0.618	0.618	1.904
5MHz	0.273	0.488	0.484	1.605
10MHz	0.127	0.275	0.279	1.096

Fig 7.3 Shows the version 3 amplitude response to frequency. Similar to the V2 The amplitude appears to be consistent until between 500 KHz and 1 MHz when it appears to tail off. The differential output is higher than that of the V2 as it has higher gain

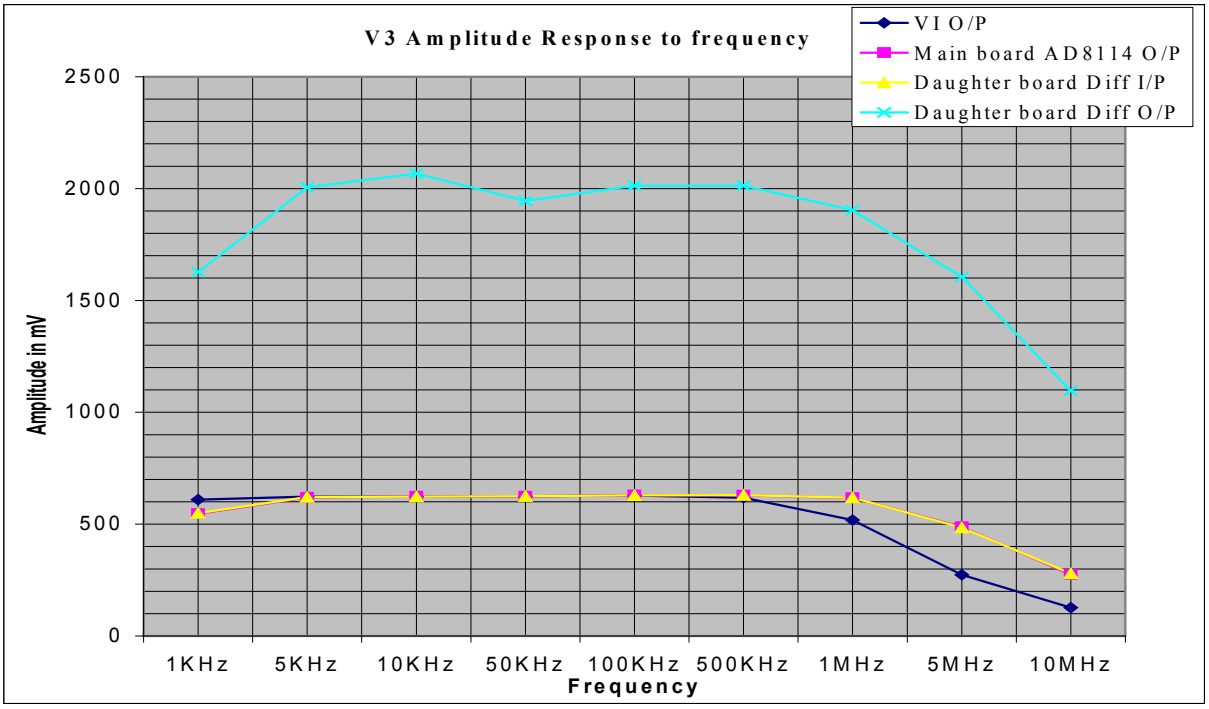

The amplitude with respect to frequency at each stage was then plotted with V2 results compared with V3 these can be seen in *Fig 7.4 – Fig 7.7*

Fig 7.4

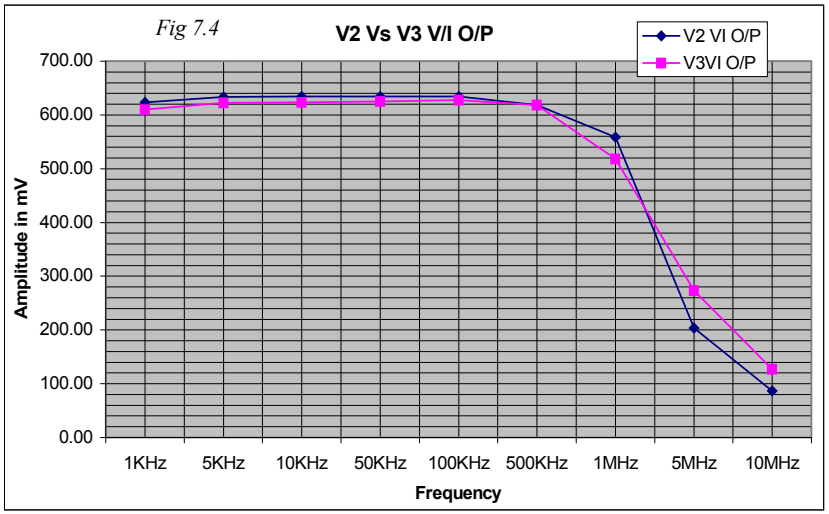

Fig 7.5

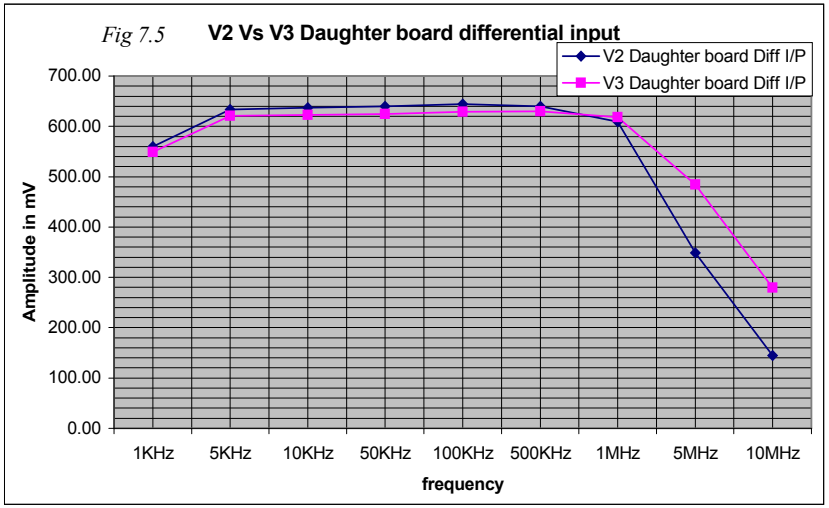

Fig 7.6

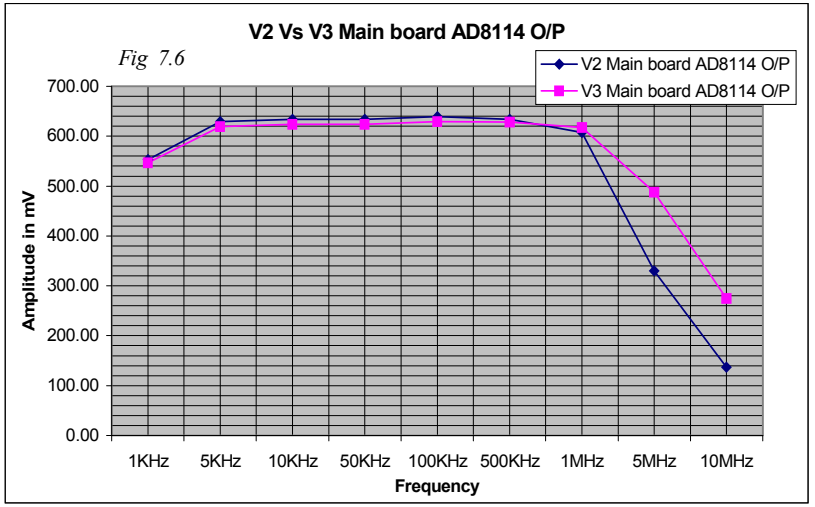

Fig 7.7

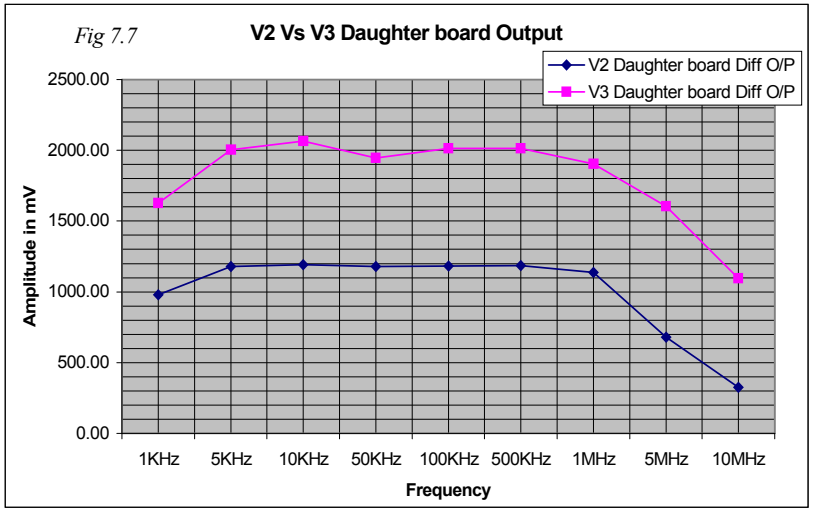

7.3.2 Noise

This experiment was set up in the same way as the previous amplitude experiment this time a 1 kHz sinusoidal was injected at the input stage of the daughter board. The results can be seen in *Table 7.3* and graphically represented in *Fig 7.8.*

Table 7.3 V2 Vs V3 With Respect to Noise at 1kHz

Noise		
Stage	**V2**	**V3**
VI O/P	0.002	0.0002
Main board ad8114 O/P	0.002	0.0003
Differential I/P	0.008	0.0004
Differential O/P	0.047	0.002

Fig 7.8 shows V2 Vs V3 with respect to noise at 1kHz, V2 generated more noise at the op amps which is then amplified in the differentiator.

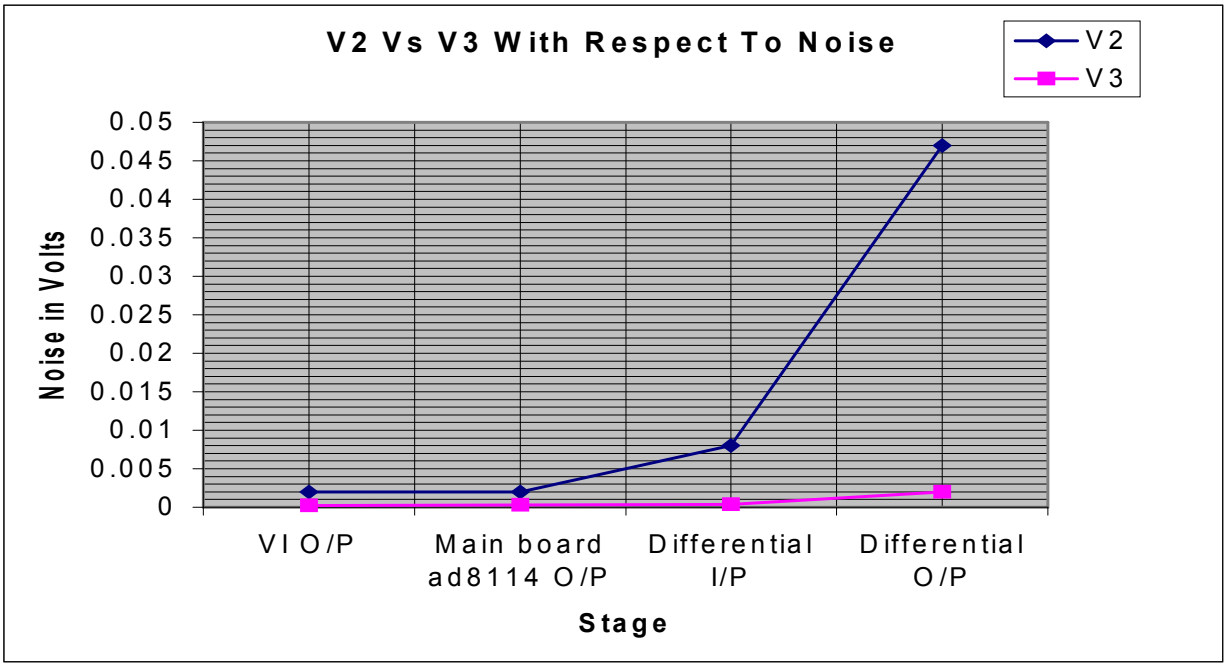

7.3.3 Signal to noise ratio

Using the results from the amplitude and noise tests and using the formula 20*Log10(V_{rms} / $Noise_{rms}$) the signal to noise ratio was calculated. These results are compared in *Table 7.4 and* graphically represented in *Fig 7.9.*

Table 7.4 V2 Vs V3 With Respect to SNR

SNR IN dB		
Stage	**V2**	**V3**
VI O/P	49.9	69.7
Main board ad8114 O/P	48.8	65.2
Differential I/P	36.9	62.7
Differential O/P	26.4	58.2

Fig 7.9 V2 Vs V3 with respect to SNR, as seen in Fig7.8 V2 generated more noise at the op amps which is then amplified in the differentiator which is why V3 has better SNR

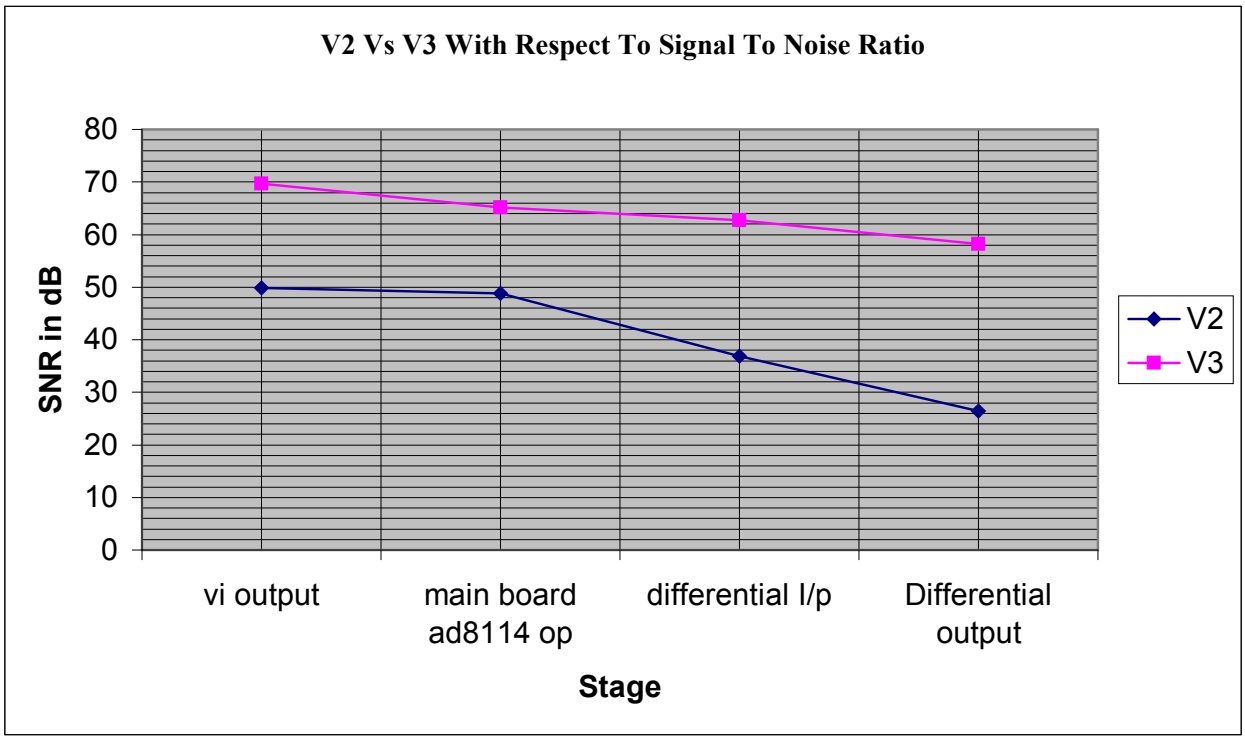

Unfortunately this only represents the SNR at 1kHz as it was not possible at the time to measure the noise levels at the higher frequencies as the software created to run the test would not allow it. As a rough guide the signal to noise ratio was calculated for all frequencies using the noise levels recorded at the 1kHz range. As certain types of noise such as thermal and shot noise are uniform over the whole frequency spectrum these calculations can show how much these types of noise are affecting the signal, however this will not represent other types of noise such as $1/f$.

It does appear from visually checking the noise in the signal during the test that there is more noise at the higher frequencies. *Table 7.5* shows the signal to noise ratio at different stages of the version 2 prototype, the most important being the differential output, which is the last stage.

Table 7.5 Signal to Noise Ratio at Different Stages of the Version 2 Prototype

Version 2				
Frequency	Signal to Noise ratio in dB			
	VI O/P	Main board AD8114 O/P	Daughter board Diff I/P	Daughter board Diff O/P
1kHz	49.869	48.818	36.901	26.382
5kHz	50.007	49.952	37.979	27.995
10kHz	50.021	50.007	38.020	28.090
50kHz	50.021	50.021	38.061	27.988
100kHz	50.021	50.075	38.115	28.017
500kHz	49.799	50.007	38.048	28.025
1MHz	48.912	49.643	37.630	27.673
5MHz	40.129	44.3496	32.794	23.220
10MHz	32.669	36.713	25.105	16.822

Table 7.6 shows the signal to noise ratio at different stages of the version 3 prototype.

Table 7.6 Signal to Noise Ratio at Different Stages of the Version 3 Prototype

Version 3				
Frequency	SNR			
	VI O/P	Main board AD8114 O/P	Daughter board Diff I/P	Daughter board Diff O/P
1kHz	69.686	65.201	62.750	58.207
5kHz	69.869	66.291	63.821	60.022
10kHz	69.869	66.361	63.849	60.286
50kHz	69.897	66.361	63.862	59.762
100kHz	69.925	66.431	63.932	60.056
500kHz	69.799	66.431	63.946	60.061
1MHz	68.266	66.277	63.779	59.573
5MHz	62.703	64.226	61.656	58.089
10MHz	56.055	59.244	56.871	54.776

From these calculations a graph was created (*Fig 7.10*) plotting the differential output signal to noise ratio across the frequency range (note the noise is calculated from the 1kHz measurements only and is only a guide).

Fig 7.10 shows the differential output signal to noise ratio across the frequency range with version 3 within the 60dB target for the majority of the frequencies.

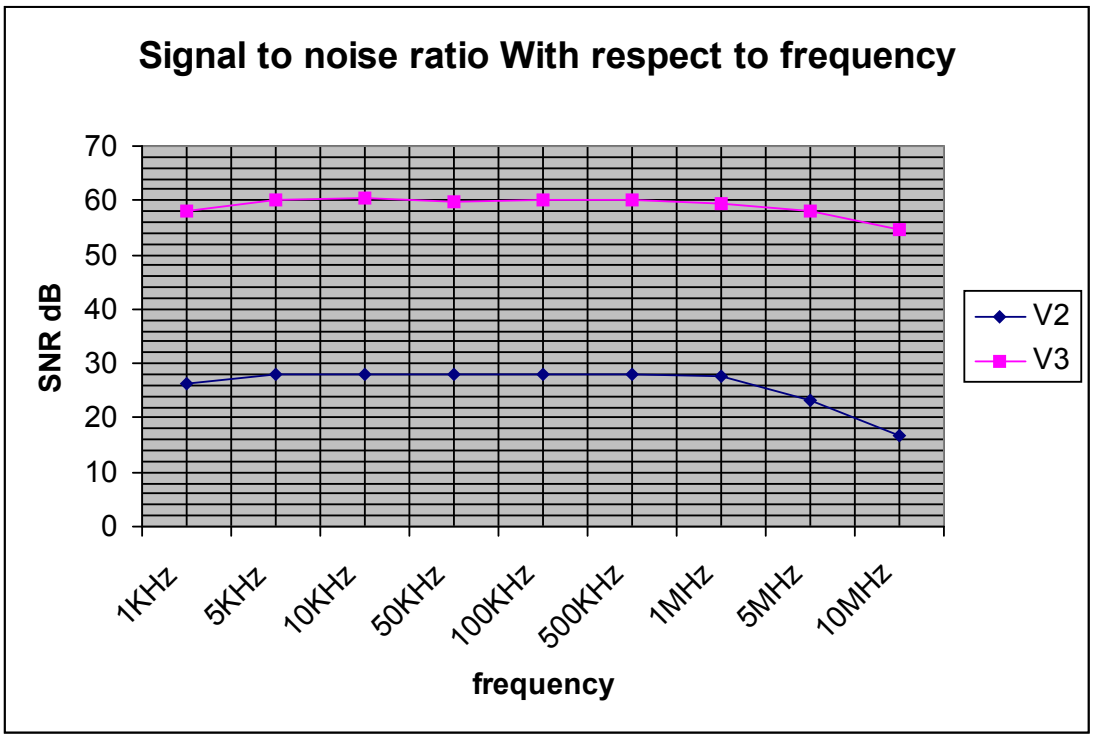

At this point in the project the full scan software and prototype housing became available. The prototypes were fitted into their water-tight housings and an organic object (in this case a potato) was scanned to see if an image could be created from them. Firstly I tested the version 2 prototype. *Fig 7.11* is a picture of the organic object in the scanner head filled with saline. *Fig 7.12* shows the resultant image obtained at a single frequency.

Fig 7.11 Organic object in the V2 prototype scanner head

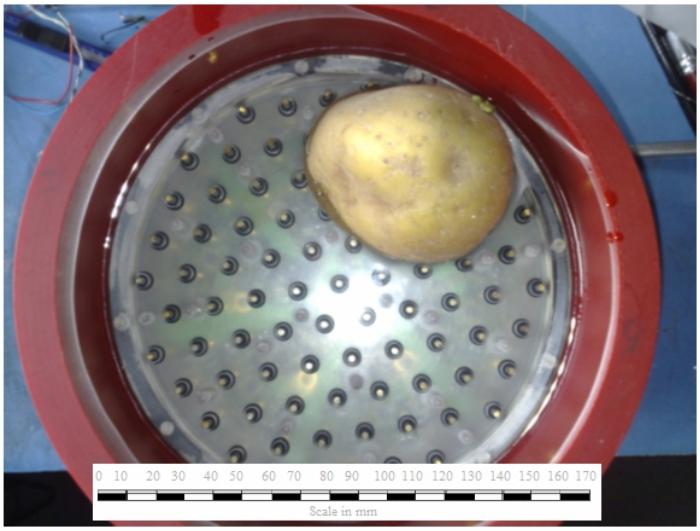

Fig 7.12 A V2 reconstructed image of the first layer (closest to the surface) scan. A representation of the potato should be clear in the top right hand corner, however due to the system having a poor SNR artefact appear throughout the image masking the scanned object

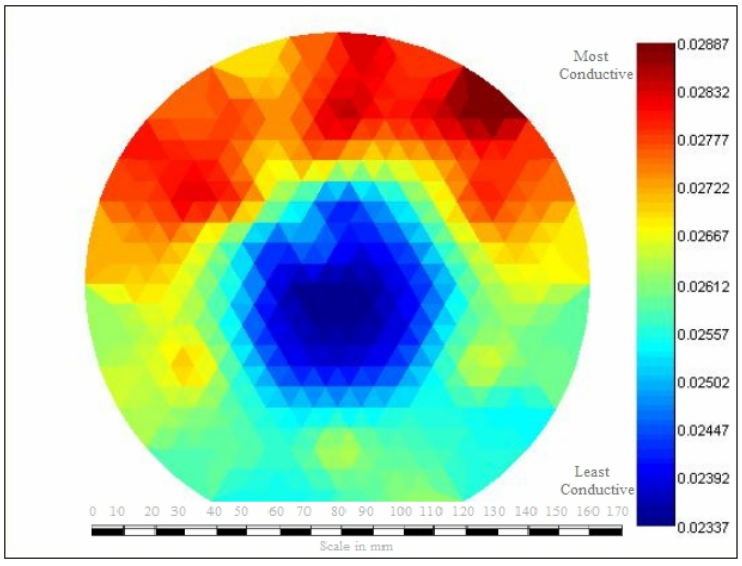

The image obtained by the V2 prototype is not very clear and is noticeably affected by the poor signal to noise ratio. *Fig 7.13* and *Fig 7.14* shows the same test with the V3 prototype.

Fig 7.13 Object in the V2 Prototype Scanner Head

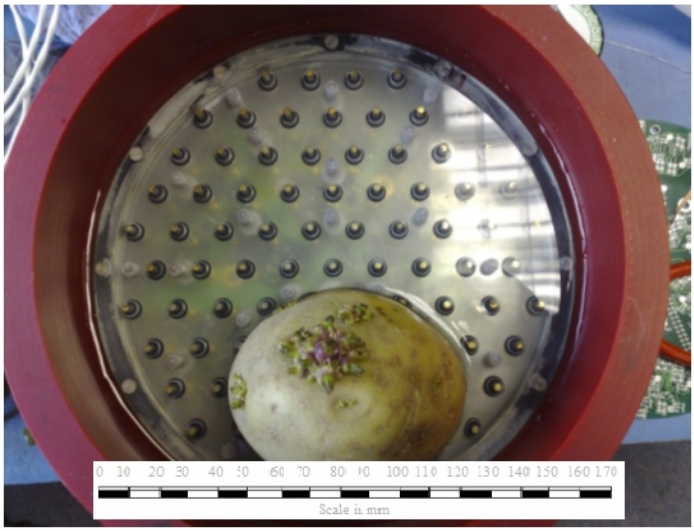

Fig 7.14 A V3 reconstructed image of the first layer scan. A representation of the potato is clear in bottom of the image which is the desired outcome.

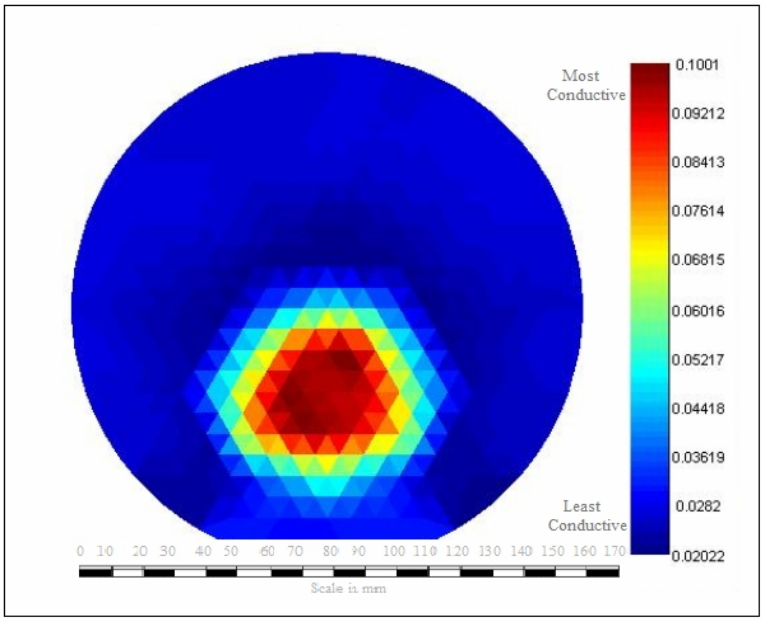

The V3 is prototype clearly produces a much clearer image. After these tests were carried out the V3 prototype was passed to the system team for a more in depth evaluation of the whole system.

8.0 Conclusion

The main objective of the project was to design and manufacture a V3 prototype with improved signal to noise ratio compared to the V2 prototype and that is able to produce a clear image of a scanned object. Initially a V2 prototype had been produced by the existing group which functionally worked but generated so much noise that it was impossible to reconstruct a clear image of a scanned object. Very little in the way of documentation was available to me at when starting this project so my first task was to reverse engineer the V2 prototype boards and generate new schematics from which to work.

Once these schematics had been generated and after an initial examination of the V2 prototype produced by the group it was clear that best practice manufacturing processes had not been used and after a discussion with the team I decided to have professionally manufactured V2 prototype boards made. These new V2 boards would then be used as the standard by which any modifications would be compared. The performance of new V2 prototype was evaluated, as expected the performance was poor, with the system having a very low signal to noise ratio, however the data gained from analysing different areas of the circuit helped identify where the performance was being affected.

In the case of the V2 prototypes large amounts of heat was being generated in the AD8114 devices used to switch the signals. This turned out to be due to the IC not being wired as specified in its datasheet. This included non used outputs not being tied to ground and incorrect power rails being used. Modifications were made to the V2 board to try and fix this issue, and the changes would be designed into the V3 prototype. The greatest contributor to noise appeared to be the op amps used to buffer the signal after the electrode this noise is then amplified later on in the differentiator. Other issues around board layout and decoupling were also highlighted.

Once the problem areas had been identified I carried out research on ways to improve the circuit. Based on research into noise reduction techniques, improvements that could be made to the problem areas highlighted during testing on the V2 board where implemented. Further performance testing was carried out, including the testing of some of the components used on the board and components that were found to increase performance were fitted, any improvements that it was not possible to incorporated for testing on the V2 prototype where designed into the V3 prototype for evaluation.

The V3 prototype boards were professionally manufactured by the same contract electronic manufacturing company as populated the components on the V2, this meant that the same manufacturing processes were performed for each and therefore any differences in performance between the V2 and V3 boards would not be influenced by the build process.

The performance of the V3 prototype was evaluated and the results showed that the signal to noise ratio of the V3 prototype has been greatly improved from that of the V2 prototype. A target was set of reaching a SNR of 60dB as this is the best the system can measure. The results show that the V3 prototype meets or exceed a SNR of 60dBs over the majority of the frequencies and only falls below that threshold when the frequency exceeds 1MHz and drops to a minimum of 54dBs at 10MHz as seen in *table 7.9.*

The system was able to perform a full scan of an object which resulted in a clearly defined and much clearer reconstructed image than it had been possible to obtain with the V2 prototype as can be seen in Fig 7.12 and 7.14. Due to these results I believe that the project can be considered as a success, however there is still room for improvement.

8.1 Future work

Further investigation to the EIM system performance needs to be performed and accurate SNR readings over the whole frequency range need to be recorded and analysed to see where improvements can be made. The EIM system needs to be integrated with the other parts of the system and phantom testing needs to be carried out and image reconstruction analysed.

References

[1] Ferlay J, Shin HR, Bray F, Forman D, Mathers C and Parkin DM. GLOBOCAN 2008 v1.2, "Cancer Incidence and Mortality Worldwide: IARC CancerBase" No. 10 [*Internet*] *http://globocan.iarc.fr/*. Lyon, France: International Agency for Research on Cancer; 2010.

[2] Howlader N, Noone AM, Krapcho M, *et al*, "SEER Cancer Statistics Review, 1975-2009" (Vintage 2009 Populations), National Cancer Institute. Bethesda, MD, *http://seer.cancer.gov/csr/1975_2009_pops09*. April 2012.

[3] B. Scholz1, R. Anderson2 On Electrical Impedance Scanning -- Principles and Simulations *1Siemens AG, Medical Engineering Group, Erlangen, Germany 2Siemens-Elema AB, Solna, Sweden* electromedica 68 – onco 2000.

[4] http://www.virtualmedicalcentre.com/health-investigation/mammography-breast-imaging/1

[5] Sharyl J. Nass, I. Craig Henderson, and Joyce C. Lashof, "Developing Technologies for the Early Detection of Breast Cancer, Mammography and Beyond:" Committee on Technologies for the Early Detection of Breast Cancer, National Cancer Policy Board, Institute of Medicine, Division of Earth and Life Studies, National Research Council NATIONAL ACADEMY PRESS Washington, DC, *http://www.nap.edu/catalog/10030.html.*

[6] Kerlikowske, K., Grady, D., Barclay, J. et al. "Effect of age, breast density, and family history on the sensitivity of first screening mammography", *JAMA, 276:33–8,* 1996.

[7] Iraj Khalkhali, Ismael Mena, Linda Diggles, "Review of imaging techniques for the diagnosis of breast cancer: a new role of prone scintimammography using technetium-99m sestamibi", *European Journal of Nuclear Medicine Eur J Nucl Med, 21:357-362*, 1994.

[8] Debbie Saslow, Carla Boetes, Wylie Burke, et al, "American Cancer Society Guidelines for Breast Screening with MRI as an Adjunct to Mammography", *CA Cancer J Clin*, 57:75–89 2007.

[9] C.W. Piccoli, Jefferson Medical College, "Contrast-enhanced breast MRI: factors affecting sensitivity and specificity, *Eur. Radiol. 7 (Suppl. 5),* S281 S288 (1997).

[10] Ajay Kapur,1 Paul L. Carson,2 Jeff Eberhard,et al. "Combination of digital mammography with semi-automated 3D breast ultrasound" *Technol Cancer Res Treat. (4): 325–334,* 2004 August.

[11] Y. Zou, Z. Guo "A review of electrical impedance techniques for breast cancer detection", *Medical Engineering & Physics 25 79–90*, 2003.

[12] Gregory Boverman, Tzu-Jen Kao, Rujuta Kulkarni,Bong Seok Kim, David Isaacson, Gary J. Saulnie and Jonathan C. Newell, "Robust Linearized Image Reconstruction for Multifrequency EIT of the Breast" , *IEEE TRANSACTIONS ON MEDICAL IMAGING, VOL. 27, NO. 10,* OCTOBER 2008

[13] Robert Hooke, Release Micrographia: *Novem.* 23. 1664, [*eBook #15491*] *ISO-8859-1* March 29, 2005

[14] PELTMR, J. C. A. (1849): in DU BOIS-REYMOND, F. 'Untersuchungen uber Tierische Elektricitat' (G. Reimer, Berlin, 1849)

[15] Hermann, Archiv fur die gesammte Physiologie vol. V and VI, ref 29, 1872

[16] GRANT *J,* "Localization of brain tumors: By determination of the electrical resistence of the growth", *jama. 81 (26)* 1923

[17] Fricke H, Morse S. The electrical capacity of tumors of the breast. *J Cancer Rev10 340–76*, 1926

[18] Geddes L A and Baker L E, "The specific resistance of biological material a compendium of data for the biomedical engineer and physiologist", *Med. Biol. Eng. 5 271–93* 1967

[19] J. C. Denniston and L. E. Baker, "Measurement of pleural effusion by electrical impedance," *Journal of Applied Physiology, vol. 38(5), pp. 851-857,* 1975

[20] R. P. Henderson and J. G. Webster, "An impedance camera for spatially specific measurements of the thorax," *IEEE Transaction on Biomedical Engineering, vol. 25(3), pp. 250-254,* 1978.

[21] Barber, D.C.; Brown, B.H. "Applied Potential Tomography". *J. Phys. E:Sci. Instrum 17: 723–733* 1984.

[22] Barber, D. C., & Seagar, A. D. "Fast reconstruction of resistance images", *Clin Phys Physiol Meas, 8 Suppl A*, 47-54, 1987.

[23] Holder, D. S. "Electrical impedance tomography (EIT) of brain function", *Brain Topogr, 5*(2), 87-93, 1992.

[24] Brown, B. H., Leathard, A. D., Lu, L., Wang, W., & Hampshire, A, "Measured and expected Cole parameters from Electrical Impedance Tomographic Spectroscopy images of the human thorax. *Physiol Meas", 16(Supp3A), 56-67*. 1995.

[25] Frerichs, I., Hahn, G., Schiffmann, H., Berger, C., & Hellige, G. "Monitoring Regional Lung Ventilation by Functional Electrical Impedance Tomography during Assisted Ventilation", *Annals New York Academy of Sciences, Apr 20(873), 493-505*, 1999.

[26] Kuen, J. W., E. J.; Seo, J. K. "Multi-frequency time-difference complex conductivity imaging of canine and human lungs using the KHU Mark1 EIT system", *Physiol Meas, 30(6), S149-164*, 2009.

[27] Li, J. H. J., C ;Faust, U (1996). "Fast EIT data acquisition system with active electrodes and its application to cardiac imaging". *Physiol. Meas., 17*, A25-A32.

[28] Henry, C. L., Phyllis, E. J., William, W. B., & Glenn, I. L. (1985). Assessment of fat-free mass using bioelectrical impedance measurements of the human body. *The American Journal of Clinical Nutrition, 41* 810-817. APRIL 1985

[29] Sadleir R and Fox R "Detection and quantification of intraperitoneal fluid using electrical impedance tomography" *IEEE Trans. Biomed. Eng. ,48 484–91,* 2001

[30] Wanjun S, Fusheng Y, Wei Z, Hongyi Z, Feng F, Xue-tao S, Ruigang L, Canjua X, Xiuzhen D and Tingyi B "Image monitoring for an intraperitoneal bleeding model of pigs using electrical impedance tomography" *Physiol. Meas. 29 217–25* 2008

[31] Tao Shang Aaron R. Hawkins, Chair Stephen M. Schultz Gregory P. Nordin Brian A. Mazzeo Adam T. Woolley. "Impedance Imaging and Measurements by Micro Probes in Aqueous Environments", Department of Electrical and Computer Engineering Brigham Young University [*Thesis*] August 2010

[32] Qin Liu1, Hun Wi1, Tong In Oh1, Eung JeWoo1 and Jin Keun Seo2 "Development of a prototype micro-EIT system using three sets of 15x8 array electrodes" Department of Biomedical Engineering, Kyung Hee University, Korea. Department of Mathematics, Yonsei University, Korea Journal of Physics: Conference Series 224 (2010) 012161

[33] Jonathan Choy and Hanching Fuh, "A Cell Impedance Measurement System" University of California, Berkeley in 2001

[34] AR Rahman, "Cell culture monitoring by impedance mapping using a multielectrode scanning impedance spectroscopy system(CellMap)" *Physiol. Meas. 29 S227,* 2008

[35] Piperno G, Frei E H and Moshitzky M, "Breast cancer screening by impedance measurements" *Frontiers Med.Biol. Eng. 2 111–17* 1990

[36] Morimoto T, Kinouchi Y, Iritani T, Kimura S, Konishi Y, Mitsuyama N, Komaki K and Monden Y "Measurement of the electrical bio-impedance of breast tumours" *Eur Surg Res. 22 86–92* 1990

[37] Wang, W., Tang, M., McCormick, M., & Dong, X., "Preliminary results from an EIT breast imaging simulation system", *Physiol Meas, 22(1), 39-48* 2001

[38] Alex Hartov1, Eugene Demidenko, Nirmal Soni1, Mariana Markova1 and Keith Paulsen1 "Using voltage sources as current drivers for electrical impedance tomography" *Meas. Sci. Technol. 13* 2002

[39] Michel Assenheimer, Orah Laver-Moskovitz, Dov Malonek, David Manor, Udi Nahaliel, Ron Nitzan1 and Abraham Saad, "The T-SCANTM technology, electrical impedance as a diagnostic tool for breast cancer detection", *Physiol. Meas. 22,* 2001

[40] Jaroslaw Stelter, Antoni Nowakowski "DIGITAL DEMODULATOR PROCEDURE FOR IMPEDANCE MAMMOGRAPHY" *18th Annual International Conference of the IEEE Engineering in Medicine and Biology Society*, Amsterdam I996.

[41] Tzu-Jen Kao, J C Newell, G J Saulnier and D Isaacson, "Distinguishability of inhomogeneities using planar electrode arrays and different patterns of applied excitation", *Physiol. Meas. 24 403–411* (2003)

[42] V. Cherepenin, A. Karpov, A. Korjenevsky, V. Kornienko, A. Mazaletskaya, D. Mazourov, and D. Meister, "A 3D electrical impedance tomography (EIT) system for breast cancer detection," *Physiol. Meas., vol. 22, 9–18,* 2001.

[43] Kim Hwa Lim, Guining Shi, Kyle McCarter, *et al, "*2D EIT FOR BIOMEDICAL IMAGING: DESIGN, MEASUREMENT, SIMULATION, AND IMAGE RECONSTRUCTION" MICROWAVE *AND OPTICAL TECHNOLOGY LETTERS / Vol. 49,* No. 12, December 2007.

[44] Skin Effect and Bio-Electrical Impedance analysis. [online] Available from rifevideos.com/pdf/skin_effect_and_bio_electrical_impedance_analysis.

[45] Peter Aberh "Skin cancer as seen by electrical impedance" Department of Laboritory Medicine Karolinska institute Stockholm, [*thesis*] 2004.

[46] Surowiec A J and Stuchly S S 1988 Dielectric properties of breast carcinoma and the surrounding tissues *IEEE Trans. Biomed. Eng vol* 35 257.

[47] KRZYSZTOF DOLOVVY, "BIOELECTROCHEMISTRY OF CELL SURFACES" *Surface Science, Vol. 15, pp. 245-366,* 1964.

[48] Michael R. Neuman BIOPOTENTIAL ELECTRODES *http://www.unc.edu/~finley/BME422/Webster/c05.pdf* Chapter 5 pp196 12/02/2008.

[49] Grimnes S "Impedance measurement of individual skin surface electrodes", *Med Biol Eng Comput*, 21, 750 – 755, 1983.

[50] Sverre Grimnes and Ørjan Grøttem Martinsen "BIOIMPEDANCE AND BIOELECTRICITY BASICS" Second Edition, ISBN: 978-0-12-374004-5.

[51] Vladimir A. Cherepenin, Alexander Y. Karpov, Alexander V. Korjenevsky, *et al, "*Three-Dimensional EIT Imaging of Breast Tissues:System Design and Clinical Testing" *IEEE TRANSACTIONS ON MEDICAL IMAGING, VOL. 21, NO. 6,* JUNE 2002.

[52] O V Trokhanova1, M B Okhapkin1 and A V Korjenevsky2 "Dual-frequency electrical impedance mammography for the diagnosis of non-malignant breast disease" *Physiol. Meas. 29 S331* 2008

[53] Bong Seok Kim1, Gregory Boverman1, Jonathan C Newell1, Gary J Saulnier and David Isaacson, "The complete electrode model for EIT in a mammography geometry" *Physiol. Meas. 28 S57* 2007

[54] Nirmal K Soni1, Alex Hartov, Christine Kogel, Steven P Poplack and Keith D Paulsen "Multi-frequency electrical impedance tomography ofthe breast: new clinical results" *Physiol. Meas. 25, 301–314*, 2004

[55] JEFFREY R. FORSYTH, "FINITE ELEMENT MESH GENERATION OF OPTICALLY CAPTURED BREAST SHAPES" Thayer School of Engineering Dartmouth College Hanover, New Hampshire [*Thesis*] MAY 2011.

[56] Halter R J, Hartov A and Paulsen K D A Broadband High-Frequency Electrical Impedance Tomography System for Breast Imaging *Biomedical Engineering, IEEE Transactions on 55 650-659*, 2008.

[57] Gary A. Ybarra, Qing H. Liu, Gang Ye, Kim H. Lim, Joon-Ho Lee, William T. Joines, and Rhett T. George, "Breast Imaging using Electrical Impedance Tomography (EIT)" Department of Electrical and Computer Engineering, Duke University, *American Scientific Publishers1– ISBN:1-58883-090-X* 2007.

[58] Gang Ye, Kim Hwa Lim, Rhett T. George Jr., Gary A. Ybarra, William T. Joines, and Qing Huo Liu "3D EIT FOR BREAST CANCER IMAGING: SYSTEM, MEASUREMENTS, AND RECONSTRUCTION" Microwave Opt Technol Lett 50: 3261–3271, 2008.

[59] Jerzy Wtorek, Jaroslaw Stelter and Antoni Nowakowski "Impedance Mammograph 3D Phantom Studies" *Department of medical and Ecological Electronics, Technical University of Gdansk, 80-952.*

.

[60] Nevis Béqo, Gerald Sze, Benjamin Tunstall, Guofeng Qiao, Ali Zarafshani and Wei Wang "A flexible and configurable hardware for the Combined EIM and Ultrasound device" *Journal of Physics: Conference Series 224,* 2010.

[61] Barber D C, Brown B H, and Freeston, I L, "Imaging Spatial Distributions of Resistivity Using Applied Potential Tomography", *Electronics Letters, 19(22), 933-935,* 1983.

[62] Yorkey, T. J., Webster, J. G., & Tompkins, W. J. Comparing reconstruction algorithms for electrical impedance tomography. *IEEE Trans Biomed Eng,* 34(11), 843-852, 1987.

[63] Gerald SZE, DETECTION OF BREAST CANCER WITH ELECTRICAL IMPEDANCE MAMMOGRAPHY [Thesis].

[64] Datasheet for Low Cost 225 MHz 16 × 16 Crosspoint Switches AD8114/AD8115 2005 Analog Devices, Inc. All rights reserved.

[65] N. Huber, W. Wang, and D.C. Barber, "Electrical Impedance Tomography" *Medical imaging principles and practices*, CNC Press Taylor & Franis Group, ISBN 978-1-4398-7102-7.

[66] J. B. Johnson, "Thermal Agitation of Electricity in Conductors" *Phys. Rev. 32, 97* (1928).

[67] H. Nyquist, Thermal Agitation of Electric Charge in Conductors pp. 110-113, Phys. Rev. 32, 110 (1928).

[68] Bruce Carter, "Op Amp Noise Theory and Applications" *Chapter 10 Literature Number SLOA082 Excerpted from Op Amps for Everyone Literature Number: SLOD006A.*

[69] W. Schottky, "Über spontane Stromschwankungen in verschiedenen Elektrizitätsleitern (spontaneous current fluctuations in different electrical conductors)" *Ann. Phys. (Leipzig) 57, 541,* 1918.

[70] W. MARSHALL LEACH, JR "Fundamentals of Low-Noise Analog Circuit Design" *IEEE Log Number 9404667, Computer Engineering, Atlanta 0018-9219/94$04.00 0 1994 IEEE* March 29, 1994.

[71] Saeed V. Vaseghi "Advanced DigitalSignal Processingand Noise Reduction. Third Edition UK"*Copyright © 2006 John Wiley & Sons Ltd, The Atrium, Southern Gate, Chichester, West Sussex PO19 8SQ, England ISBN-13 978-0-470-09494-5 (HB) ISBN-10 0-470-09494-X (HB).*

[72] I2C® CMOS 8 × 12 Unbuffered Analog Switch Array With Dual/Single Supplies.

[73] OPA657SBOS197E – DECEMBER 2001 – REVISED DECEMBER 2008

1.6GHz, Low-Noise, FET-Input OPERATIONAL AMPLIFIER
www.ti.comCopyright © 2001-2008, Texas Instruments Incorporated.

[74] Paul Horowitz, Winfield Hill, 1989, *The Art of electronics second edition, Cambridge University press, ISBN 0-521-37095-7* chapter 7 pp 456-457.

[75] Tim Williams, 1996,EMC for production designers second edition, Reed Educational and professional publishing LTD, ISBN 0 7506 2466 3 pp 115, 156-157, 233.

[76] Bruce Carter , "Amplifiers": *Analog Applications Journal August 2000 Analog and Mixed-Signal Products 47* Op Amps Texas Instruments Incorporated The PCB is a component of op amp.

[77] Douglas Brooks "Splitting Planes For Speed and Power" *Printed Circuit Design, a CMP Media publication, December, 2000 2000 CMP Media, Inc. 2001 UltraCAD Design, Inc. http://www.ultracad.com*

[78] John Ardizzoni, A practical guide to high speed circuit board layout, *Analogue dialog 39*-09 september 2005

Appendix

Fig 9.0 Diagram depicting the new PCB layout. The Gerber's for each layer can be found overleaf

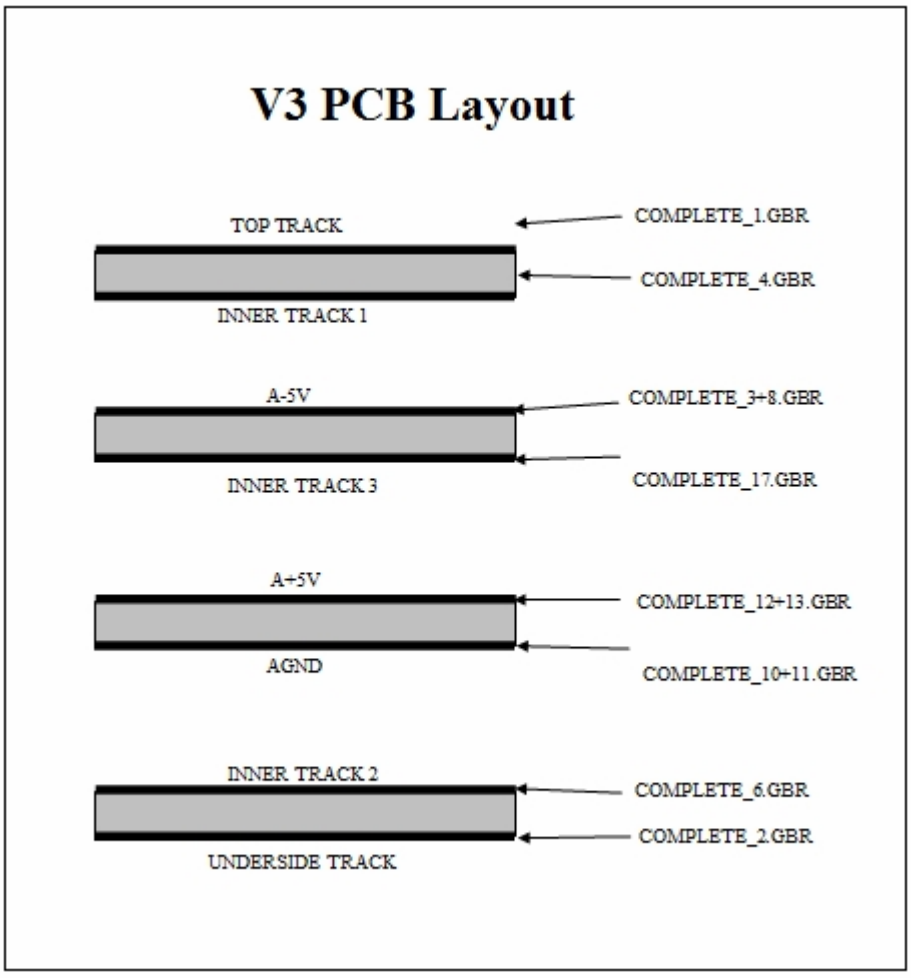

Fig 9.1 Top track layer

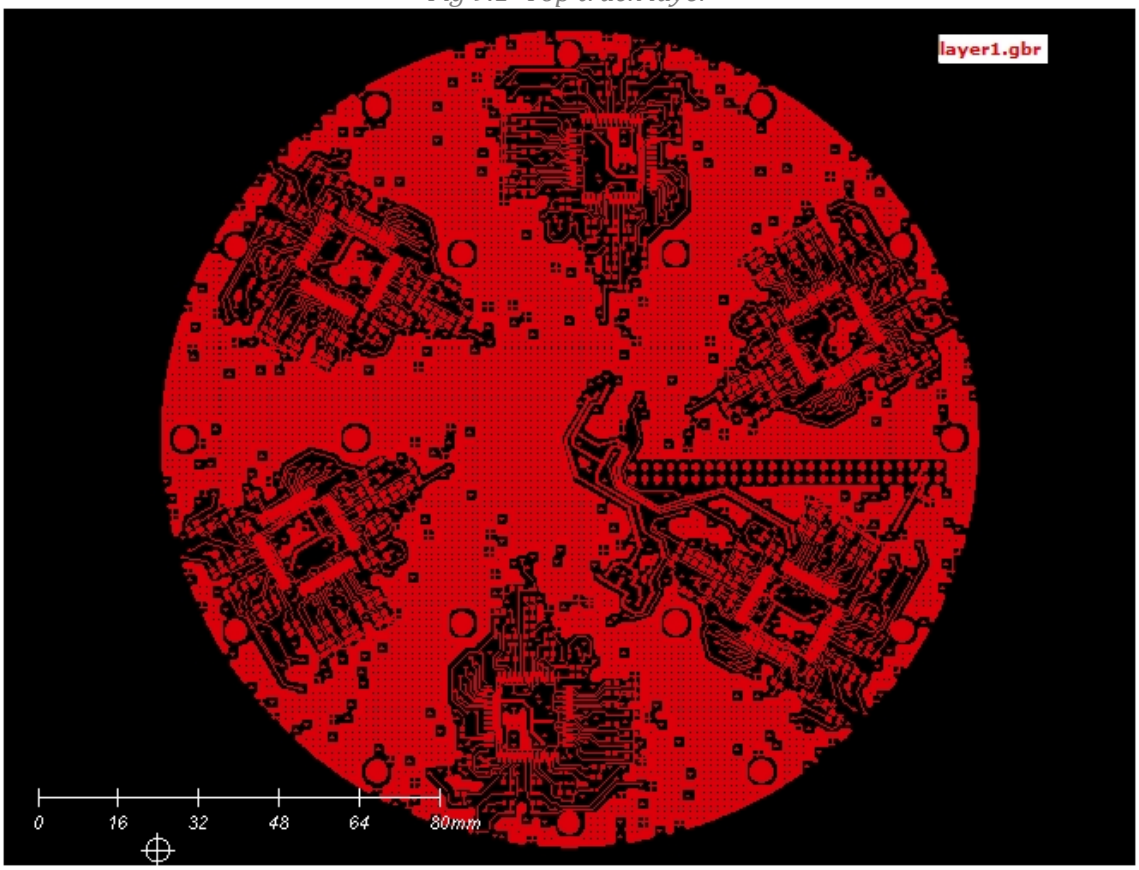

Fig 9.2 analogue ground plane

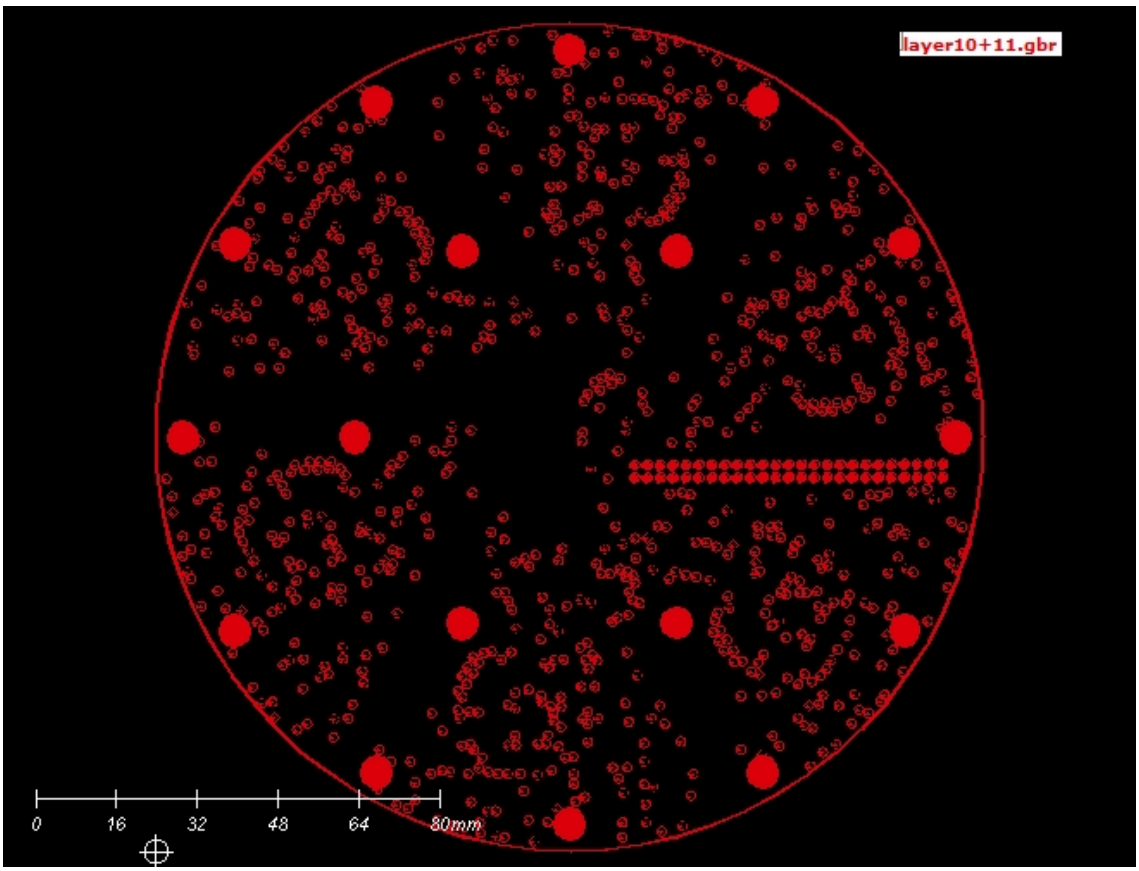

Fig 9.3 +5V analogue plane

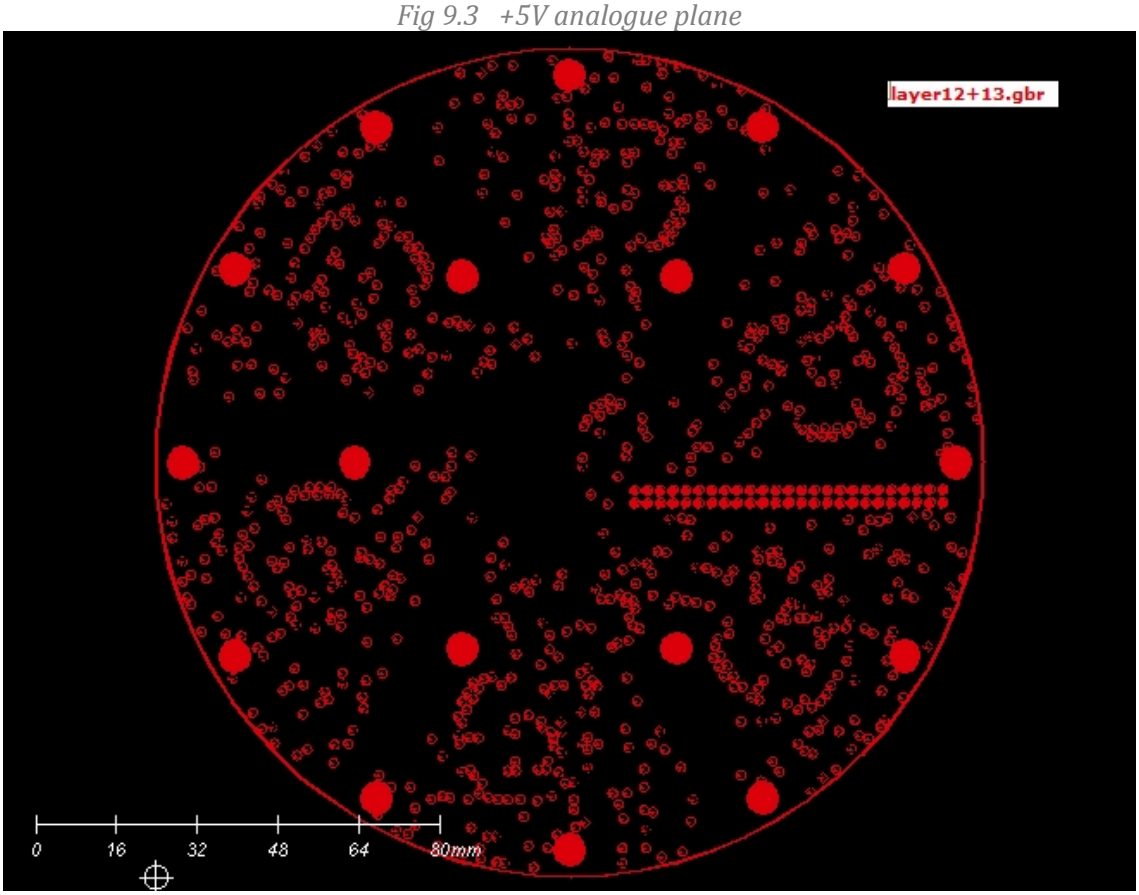

Fig 9.4 Inner track 3

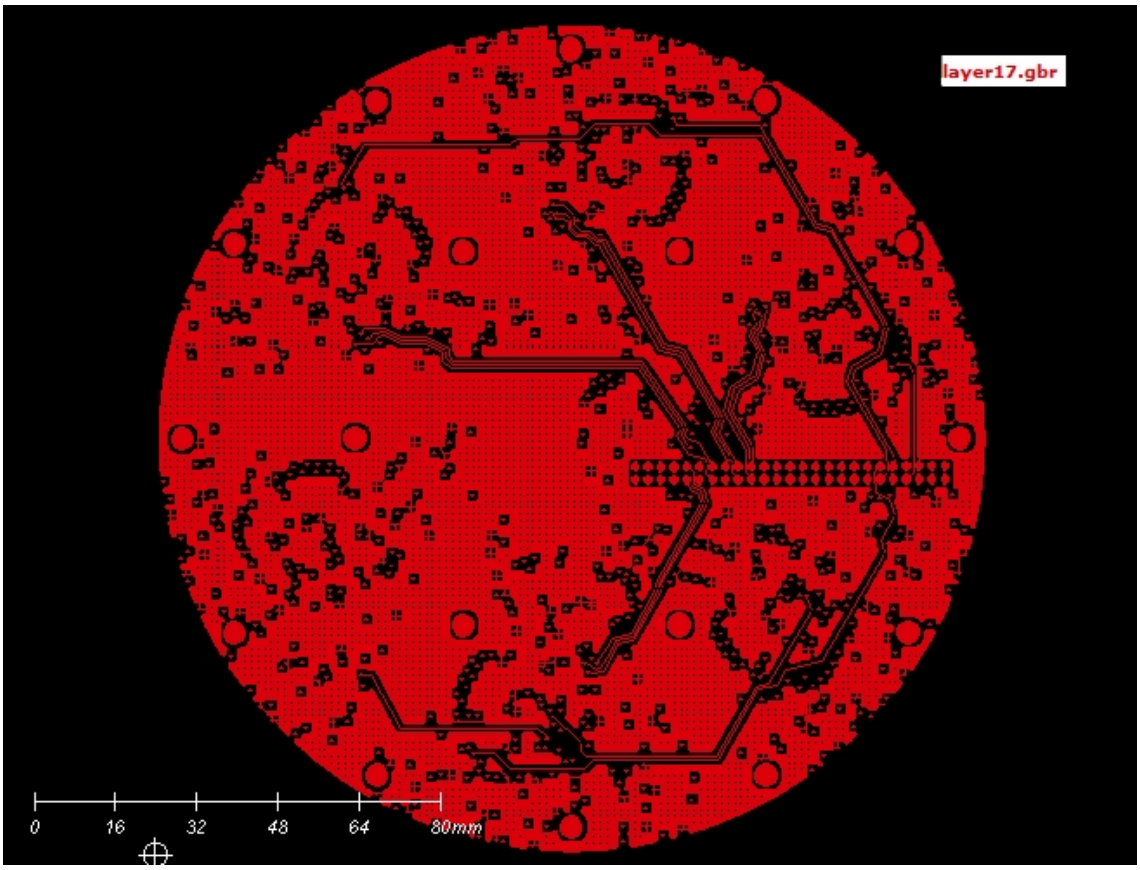

Fig 9.5 bottom track layer

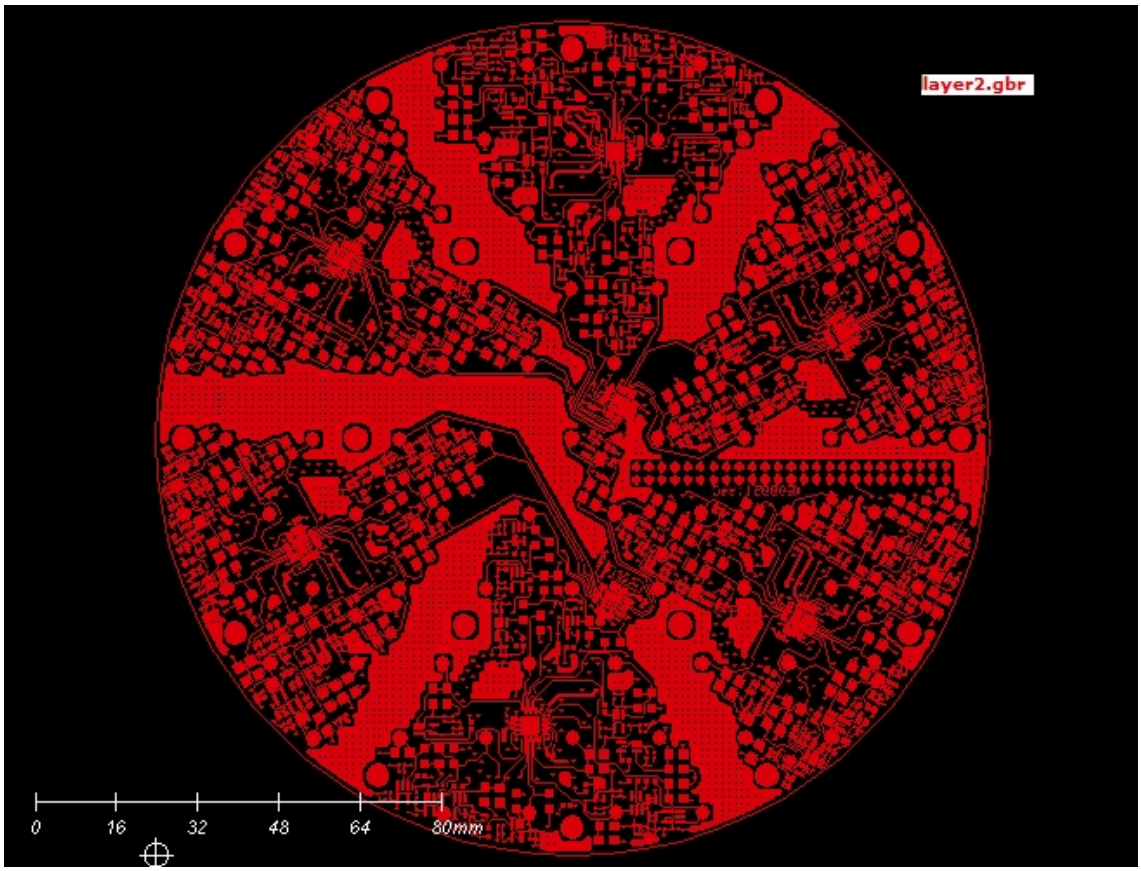

Fig 9.6 -5V analogue plane

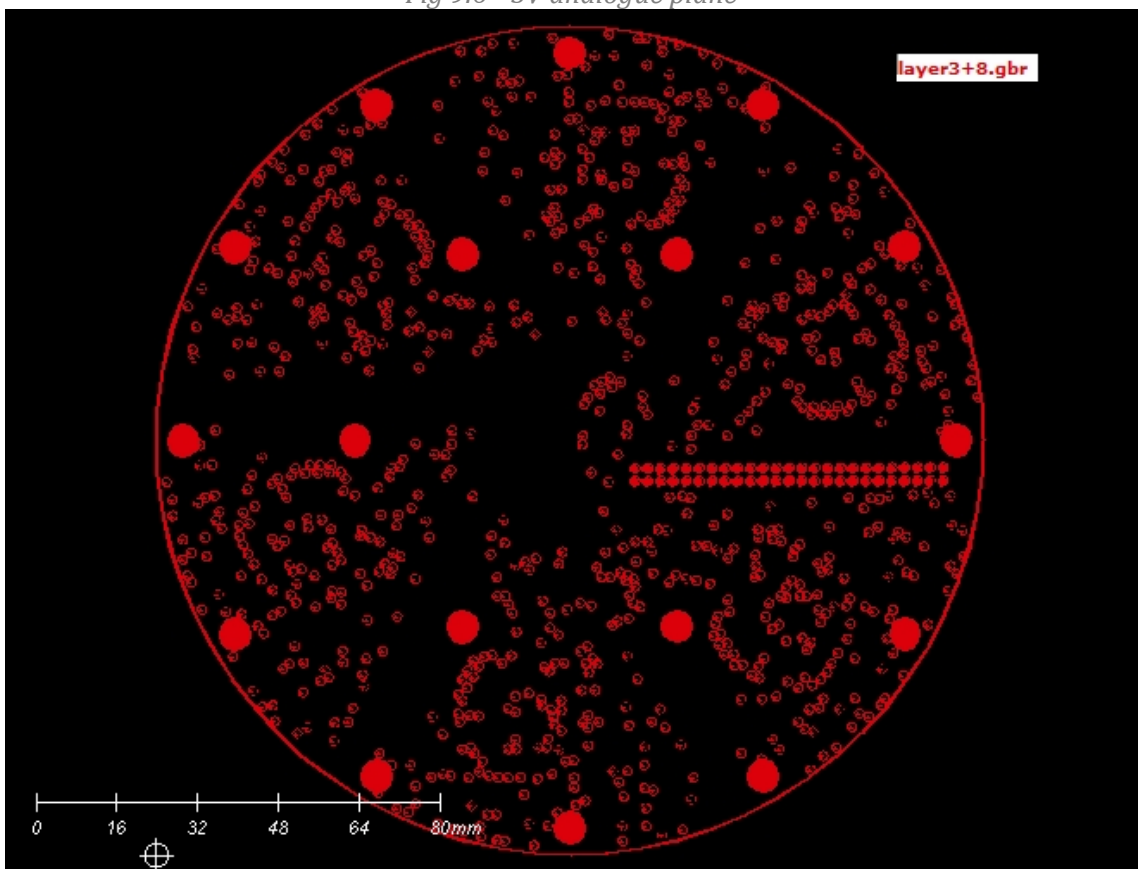

Fig 9.7 Inner track 1

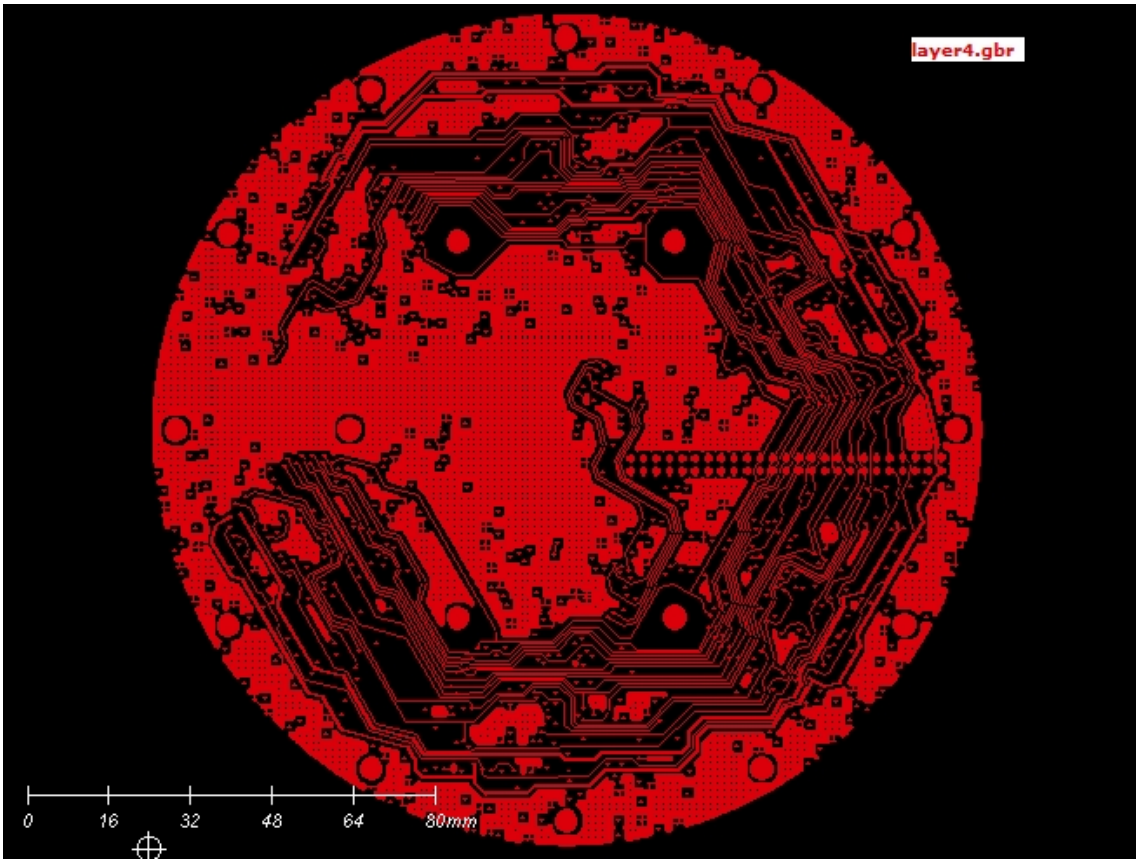

Fig 9.8 Inner track 2